Received: *February 4, 2000*, Accepted: *April 5, 2000*

Parton-shower simulations of R-parity violating supersymmetric models

Herbert Dreiner and Mike H. Seymour

Rutherford Appleton Laboratory, Chilton, Didcot OX11 0QX, UK
E-mail: dreiner@v2.rl.ac.uk, m.seymour@rl.ac.uk

Peter Richardson

Department of Physics, Theoretical Physics, University of Oxford
1 Keble Road, Oxford OX1 3NP, UK
E-mail: p.richardson1@physics.ox.ac.uk

Abstract: We study the colour connection structure of R-parity violating decays and production cross sections, and construct a Monte Carlo simulation of these processes including colour coherence effects. We then present some results from the implementation of these processes in the HERWIG Monte Carlo event generator. We include the matrix elements for the two-body sfermion and three-body gaugino and gluino decays as well as the two-to-two resonant hard production processes in hadron-hadron collisions.

Keywords: Supersymmetric Standard Model, QCD, Hadronic Colliders.

Contents

1. Introduction

In the past few years there has been a large amount of interest in R-parity violating ($\not{R}_p$) supersymmetric (SUSY) models, motivated by the possible explanations of various experimental discrepancies, e.g. [1]–[9]. It has become clear that if we are to explore all possible channels for the discovery of supersymmetry then $\not{R}_p$ models must be investigated. For a recent review on R-parity violation see [10].

In the Minimal Supersymmetric Standard Model (MSSM) a discrete multiplicative symmetry, R-parity (R_p) is imposed,

$$R_p = (-1)^{3B+L+2S}\,, \tag{1.1}$$

where B is the baryon number, L the lepton number and S the spin of the particle. All the Standard Model particles have $R_p = +1$ and their super-partners have $R_p = -1$. The conservation of R-parity forbids the terms in the superpotential which violate baryon or lepton number[1]

$$\mathbf{W}_{\not{R}_p} = \frac{1}{2}\lambda_{ijk}\,\varepsilon^{ab}L^i_a L^j_b \overline{E}^k + \lambda'_{ijk}\,\varepsilon^{ab}L^i_a Q^j_b \overline{D}^k + \frac{1}{2}\lambda''_{ijk}\,\varepsilon^{c_1c_2c_3}\overline{U}^i_{c_1}\overline{D}^j_{c_2}\overline{D}^k_{c_3} + \kappa_i L_i H_2\,, \tag{1.2}$$

where $i,j,k = 1,2,3$ are the generation indices, $a,b = 1,2$ are the $SU(2)_L$ indices and $c_{1,2,3} = 1,2,3$ are the $SU(3)_C$ indices. $L^i(Q^i)$ are the lepton (quark) SU(2) doublet superfields, $\overline{E}^i$ ($\overline{D}^i, \overline{U}^i$) are the electron (down and up quark) SU(2) singlet superfields, and H_n, $n = 1,2$, are the Higgs superfields. We shall neglect the last term in eq. (1.2) which mixes the lepton and Higgs SU(2) doublet superfields. For a recent summary of the bounds on the couplings in eq. (1.2) see [11].

This superpotential gives interactions which violate either lepton or baryon number. For example the first term will give interactions of a slepton and two leptons which violates lepton number. The third term gives an interaction of two quarks and squark, which violates baryon number. When combined with the MSSM superpotential there are also terms involving the interactions of three sleptons/squarks and a Higgs which violate either lepton or baryon number.

[1] It should be noted that some authors choose to define this superpotential without the factors of one half in the LLE and UDD terms. This will lead to differences in the Feynman rules, but the results with this second convention can always be obtained by taking λ or λ'' to be twice their value in our convention.

R_p is imposed in the MSSM to avoid the simultaneous presence of the second two terms in eq. (1.2). These lead to fast proton decay, in disagreement with the experimental lower bounds on the proton lifetime. However in order to guarantee proton stability it is sufficient to forbid only one set of these terms. This is achieved for example by lepton parity

$$
\begin{aligned}
(L^i, \bar{E}^i) &\rightarrow -(L^i, \bar{E}^i)\,, \\
(Q^i, \bar{U}^i, \bar{D}^i, H_1, H_2) &\rightarrow (Q^i, \bar{U}^i, \bar{D}^i, H_1, H_2)\,,
\end{aligned} \tag{1.3}
$$

which allows the third term in eq. (1.2) but forbids the remaining terms. Thus baryon number is violated ($\not{B}$) but lepton number is conserved and the proton is stable. Similarly there are symmetries such that lepton number is violated and baryon number is conserved. This also prevents proton decay. Both cases lead to very different phenomenology from the MSSM.

In the MSSM the conservation of R_p implies that

1. Sparticles are produced in pairs.

2. The lightest supersymmetric particle (LSP) is stable.

3. Cosmological bounds on electric- or colour-charged stable relics imply that a stable LSP must be a neutral colour singlet [12].

However, in the case of $\not{R}_p$ models we can have

1. Single sparticle production.

2. The LSP can decay. As the LSP is unstable it does not have to be a neutral colour singlet. It can be any supersymmetric particle.

3. Lepton or baryon number is violated.

In the MSSM, as the LSP is stable, the experimental signatures of SUSY processes typically involve missing transverse energy in collider experiments. However, if R-parity is violated, and the LSP decays in the detector, the missing energy signatures of the MSSM no longer apply or are severely diluted. It therefore requires a different experimental search strategy. In particular, in the $\not{B}$ case, where the final state is predominantly hadronic, it may be hard to extract a signal over the QCD background in hadron colliders.

Despite the interest in $\not{R}_p$ and the potential experimental problems, there have been few experimental studies at hadron colliders. The first systematic study of $\not{R}_p$ signatures at hadron colliders was presented in [13]. More recent overviews of the search potential at the LHC and Run II of the Tevatron have been presented in [14, 15]. These studies have been limited by the fact that few simulations have been available. In hadron-hadron collisions the only available Monte Carlo event generator is ISAJET [16] where the $\not\!R_{\rm p}$ decays can be implemented using the `FORCE` command, i.e. the decay mode of a given particle, e.g. the LSP, can be specified by hand. However there has been no simulation which includes all the decay modes and the single sparticle production processes.

Here we present the calculations required to produce a Monte Carlo event generator for the two-body sfermion and three-body gaugino and gluino $\not\!R_{\rm p}$ decay modes as well as all two-to-two $\not\!R_{\rm p}$ resonant production processes in hadron-hadron collisions. We have only included those production processes where a resonance is possible, so for example processes which can only occur via a t-channel diagram are not included. However where a process can occur via a resonance all the diagrams including non-resonant s-channel and t-channel diagrams have been included. We also discuss colour coherence effects via the angular ordering procedure (which we describe in detail below), and some preliminary results from the implementation of these processes in the HERWIG Monte Carlo event generator [17]. In R-parity violating processes we see a new type of vertex which couples three particles in the fundamental representation of SU(3) and violates baryon number. The colour structure of these processes is very different to that seen in the Standard Model or MSSM where the colour structure can be simplified by letting, $N_c \to \infty$, where N_c is the number of colours. However these new vertices which violate baryon number can only exist for $N_c = 3$. Details of the implementation of supersymmetric processes with and without $\not\!R_{\rm p}$ can be found in [18].

After a general discussion of the angular ordering procedure in the Standard Model in section 2 we discuss the extension to the $\not\!R_{\rm p}$ decays and hard production processes in section 3. In section 4 we describe the hadronization procedure which we adopt for the $\not\!R_{\rm p}$ processes.

We then present some preliminary results of the Monte Carlo simulation in section 5. We have made new calculations of all the necessary matrix elements, and include them as an appendix.

JHEP04(2000)008

2. Monte Carlo simulations

In general a Monte Carlo event generator, for a process involving at least one hadron, consists of three parts.

1. A hard scattering process, either of the incoming fundamental particles in lepton collisions or of a parton extracted from a hadron in hadron initiated processes.

2. A parton-shower phase where the partons coming into or leaving the hard process are evolved according to perturbative QCD.

3. A hadronization model in which the partons left at the end of the parton-shower phase are formed into the hadrons which are observed. For processes with hadrons in the initial state after the removal of the partons in the hard process we are left with a hadron remnant. This remnant is also formed into hadrons by the hadronization model.

We now discuss these three stages in turn.

2.1 Hard scattering

The hard scattering process is described by a matrix element calculated to a fixed order in perturbation theory, usually only leading order. The momenta of the particles involved in the collision can then be generated according to the matrix element. The Monte Carlo event generator then needs to take the results of this perturbative calculation, at a high scale, and generate the hadrons which are observed.

2.2 Parton shower

In a scattering process the incoming or outgoing partons can emit QCD radiation, e.g. $q \to gq$ and $g \to gg$, or split into quark-antiquark pairs, $g \to q\bar{q}$. A full perturbative treatment of this part of an event is not possible. (If it were possible it would be included in the hard scattering matrix element.) We must therefore make an approximation and focus on the dominant contributions in the showering process. The emission of QCD radiation is enhanced for (a) Collinear emission and for (b) Soft emission. We discuss these two below in more details. Our approximation will consist in focusing on these enhanced regions of radiation. We then discuss this in an explicit example.

(a) **Collinear emission.** If we consider the emission of QCD radiation in the collinear limit then, after azimuthal averaging, the *cross-section* obeys a factorization theorem [19]. This can be understood as follows, the cross section for a process in which one parton pair is much more collinear than any other pair can be written as the convolution of a universal, i.e. process independent, splitting function and the cross section for the same process where the collinear pair is replaced by a single parton of the corresponding flavour. Due to this functional form we can then apply this procedure to the next most collinear pair in the final state, and so on. We thus have an iterative rule which leads to a description of multi-parton final states as a Markov chain [19]. This can be viewed as an evolution in some energy-like scale, such as the virtuality, where a parton at high scale is evolved by successive branchings to a lower scale. However, the collinear factorization does not specify what the evolution variable should be, i.e. it has the same form for any variable proportional to the virtuality, e.g. the transverse momentum. This iterative procedure then correctly resums the leading collinear singularities to all orders in perturbation theory [19].

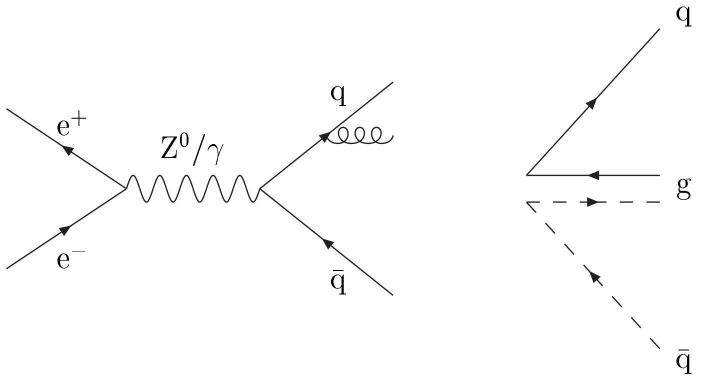

Figure 1: Feynman diagram and colour flow for $e^+e^- \to q\bar{q}g$.

(*b*) **Soft emission.** For the emission of QCD radiation in the soft limit, a factorization theorem exists for the *amplitude* of the process. The amplitude for a process in which one gluon is much softer than the other energy scales in the process can be written as a product of a universal eikonal current and the amplitude for the same process without the soft gluon. After we square the amplitude and sum over the spins of the external partons, we obtain a result which depends on the momenta of all the external partons. It therefore seems unlikely that a Markov description based on sequential parton splittings can be recovered. The surprising result [20, 21] is that, after azimuthal averaging, these effects *can* be incorporated into a collinear algorithm by using the correct choice for the evolution scale, namely the opening angle.

2.2.1 Example: $e^+e^- \to q\,\bar{q}\,g\,g$

We can illustrate this with a simple example, i.e. the process $e^+e^- \to q\,\bar{q}\,g_1$, shown in figure 1. The semi-classical eikonal current can be used to study the emission of an extra soft gluon in this process, i.e. the process $e^+e^- \to q\,\bar{q}\,g_1\,g_2$ where the second gluon is much softer than the other partons. The matrix element including the emission of the extra soft gluon is given by

$$\mathbf{M}(k_1, k_2, p_1, p_2, p_3; q) = g_s \mathbf{m}(k_1, k_2, p_1, p_2, p_3) \cdot \mathbf{J}(q)\,, \tag{2.1}$$

where

- $\mathbf{m}(k_1, k_2, p_1, p_2, p_3)$ is the tree-level amplitude for the underlying process, $e^+(k_1)e^-(k_2) \to q(p_1)\bar{q}(p_2)g_1(p_3)$.
- $\mathbf{M}(k_1, k_2, p_1, p_2, p_3; q)$ is the matrix element for the process $e^+(k_1)e^-(k_2) \to q(p_1)\,\bar{q}(p_2)\,g_1(p_3)\,g_2(q)$, i.e. including the emission of an extra soft gluon, g_2, with momentum q.

- $\mathbf{J}(q)$ is the non-abelian semi-classical current for the emission of the soft gluon with momentum q, from the hard partons.

- g_s is the strong coupling constant.

Explicitly in our example, the current, $\mathbf{J}(q)$, is given by [21]

$$\mathbf{J}(q) = \sum_{s=1,2} \mathbf{J}^{b,\mu}(q)\varepsilon_{\mu,s}\,, \tag{2.2}$$

where $\varepsilon_{\mu,s}$ is the polarization vector of the gluon and

$$\mathbf{J}^{b,\mu}(q) = \mathbf{t}^{b,\mathrm{q}}_{c_1c'_1}\,\mathbf{t}^{a}_{c'_1c_2}\left(\frac{p_1^\mu}{p_1\cdot q}\right) + \mathbf{t}^{a}_{c_1c'_2}\,\mathbf{t}^{b,\bar{\mathrm{q}}}_{c'_2c_2}\left(\frac{p_2^\mu}{p_2\cdot q}\right) + if^{aa'b}\,\mathbf{t}^{a'}_{c_1c_2}\left(\frac{p_3^\mu}{p_3\cdot q}\right), \tag{2.3}$$

where $\mathbf{t}^{b,q}$ and f^{abc} are the SU(3) colour generators in the fundamental representation and adjoint representations respectively.

Radiation functions. We now define the radiation functions of [22]. This will allow us to express the square of the current, eq. (2.3), in a useful way. First we define the dipole radiation function $W_{ij}(\Omega_q)$, which describes the radiation of a soft gluon, with momentum q, from a pair of partons i and j. Note that $W_{ij}(\Omega_q)$ only depends on the direction of q, Ω_q, and not its energy.

$$\frac{2}{\omega^2}W_{ij}(\Omega_q) \equiv -\left(\frac{p_i}{p_i\cdot q} - \frac{p_j}{p_j\cdot q}\right)^2 = \frac{2}{\omega^2}\left(\frac{\xi_{ij}}{\xi_i\,\xi_j} - \frac{1}{2\gamma_i^2\,\xi_i^2} - \frac{1}{2\gamma_j^2\,\xi_j^2}\right), \tag{2.4}$$

where

- ω is the energy of the soft gluon,

- $\xi_{ij} = p_i\cdot p_j/E_iE_j = 1 - v_iv_j\cos\theta_{ij}$,

- $\xi_i = 1 - v_i\cos\theta_i$,

- $\gamma_i = E_i/m_i = 1/\sqrt{1-v_i^2}$,

- v_i is the velocity of parton i,

- θ_i is the angle between the direction of motion of the soft gluon and the parton i,

- θ_{ij} is the angle between the partons i and j.

We can now use the dipole radiation functions to express the current squared for a given process in the following form:

$$\mathbf{J}^2(q) = \frac{C_{\mathbf{m}}}{\omega^2}W(\Omega_q)\,, \tag{2.5}$$

where C_m is the colour factor for the tree-level process, and $W(\Omega_q)$ the radiation pattern, given below in terms of the dipole radiation functions. For the process $e^+e^- \to q\bar{q}g$ the colour factor $C_m = C_F N_c$ and the radiation pattern is given by

$$W_{q\bar{q}g}(\Omega_q) = C_A[\, W_{qg}(\Omega_q) + W_{\bar{q}g}(\Omega_q)\,] - \frac{1}{N_c} W_{q\bar{q}}(\Omega_q)\,, \tag{2.6}$$

where $C_F = (N_c^2-1)/(2N_c)$ and $C_A = N_c$ are the Casimirs of the fundamental and adjoint representations respectively, with an arbitrary number of colours N_c. This corresponds to emission of the soft gluon from colour dipoles, i.e. W_{qg} is emission from the dipole formed by the quark and the anticolour line of the gluon, $W_{\bar{q}g}$ emission from the colour line of the gluon and the antiquark and $W_{q\bar{q}}$ emission from the quark and antiquark. Note that the $q\bar{q}$ dipole is negative which is a problem if we wish to use a probabilistic approach to treat the soft gluon radiation.

The dipole radiation function can then be split into two parts as was done in [22], i.e.

$$W_{ij}(\Omega_q) = W_{ij}^i(\Omega_q) + W_{ij}^j(\Omega_q)\,, \tag{2.7}$$

where

$$W_{ij}^i = \frac{1}{2\xi_i}\left(1 - \frac{1}{\gamma_i^2\xi_i} + \frac{\xi_{ij}-\xi_i}{\xi_j}\right). \tag{2.8}$$

The function W_{ij}^i has the following properties:

- After averaging over the azimuthal angle of the soft gluon about the parton i it corresponds to emission in a cone about the direction of the parton i up to the direction of j, [20, 21].
- If the parton i is massive then soft radiation in the direction of the parton is reduced, i.e. emission within an angle of order $\theta \sim m_i/E_i$ is suppressed, [22].
- In the massless limit it contains the collinear singularity as $\theta_i \to 0$, [22], but has no collinear singularity as $\theta_j \to 0$.
- While W_{ij}/ω^2 is Lorentz invariant the individual functions W_{ij}^i/ω^2 and W_{ij}^j/ω^2 are not.

This allows us to rewrite the square of the current, eq. (2.3), in the following form, using these radiation functions, as

$$\begin{aligned} W_{q\bar{q}g}(\Omega_q) = {} & 2C_F\left(W_{qg}^q + W_{\bar{q}g}^{\bar{q}}\right) + C_A\left(W_{g\bar{q}}^g + W_{gq}^g\right) + \\ & + N_c^{-1}\left(W_{qg}^q - W_{q\bar{q}}^q + W_{\bar{q}g}^{\bar{q}} - W_{\bar{q}q}^{\bar{q}}\right), \end{aligned} \tag{2.9}$$

which should be inserted in eq. (2.5). This gives our main result in this example. The last term in eq. (2.9), and other terms of this type, can be neglected as it is suppressed by $1/N_c^2$ with respect to the leading order term, as $C_F,\ C_A \propto N_c$, and is also dynamically suppressed as it does not contain a collinear singularity in the

JHEP04(2000)008

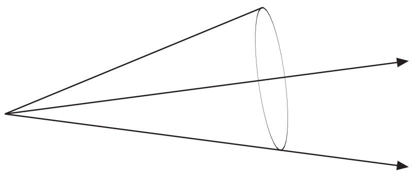

Figure 2: Emission in angular ordered cones.

massless limit (e.g. the singularity in the quark direction cancels between the W^q_{qg} and $W^q_{q\bar{q}}$ terms). Thus part of our approximation for the parton shower will consist of dropping the $1/N_c^2$ terms.

Colour connected partons. We can now define the concept of the colour connected parton. Two partons are considered to be colour connected if they share the same colour line. The colour flow, in the large N_c limit, for the process $\mathrm{e^+e^-} \to \mathrm{q\bar{q}g}$ is shown in figure 1 with a dashed and a solid line. Thus the $\mathrm{\bar{q}}$ and g are colour connected and the q and g are colour connected, while the $\mathrm{\bar{q}}$ and q are not colour connected. Each quark only has one colour connected partner in a given Standard Model Feynman diagram and each gluon has two. Colour connected partners are defined at each stage of the iterative parton showering procedure. If the final state q were to emit another gluon, $\mathrm{g_2}$, the new final state q would be colour connected to $\mathrm{g_2}$ and no longer to g. g and $\mathrm{g_2}$ would then also be colour connected.

Angular ordered emission and colour coherence. We see from eq. (2.9) that neglecting the final term, using the properties of the function W^i_{ij}, and averaging over the azimuthal angle of the gluon about a parton, the radiation can only occur in a cone about the direction of the parton up to the direction of its colour partner. This is shown in figure 2. We can draw a cone around parton one with half-angle given by the angle between the momenta of partons one and two. The emission from parton one within the cone defined by its colour connected partner, parton two, is called angular ordered emission.

The angular ordering procedure is one way of implementing the phenomenon of colour coherence. The idea of colour coherence is that if we consider a large angle gluon it can only resolve the total colour charge of a pair of smaller angle partons, and not their individual charges. It is therefore as if the larger-angle soft gluon was emitted before the smaller angle branchings. There have been a number of experimental studies of colour coherence effects. In particular the string effect in $\mathrm{e^+e^-}$ collisions [23], where there is a suppression of soft QCD radiation between the two quark jets in three jet events. There have also been studies of colour coherence effects between the initial and final states in hadron-hadron collisions, [24, 25]. It is now firmly established that event generators that do not incorporate colour coherence cannot reliably predict the hadronic final state.

Although we have averaged over the azimuthal angle of the emission of the gluon in both the soft and collinear cases, azimuthal effects, e.g. due to spin correlations, can be included [26], after the full parton shower has been generated.

2.2.2 Non-planar colour flows

We have explained in an example how the cross section for $n+1$ partons factorizes in both the collinear and soft limits into a universal splitting term and the cross section for n partons. Both of these limits can be implemented by using angles as the evolution variable in a Markov branching procedure. We start at the hard cross-section, normally with a two-to-two process. The maximum angle of emission from a parton is set by the direction of the colour partner. We then generate some smaller angle parton, e.g. a gluon from a quark. Then we repeat the procedure, i.e. the gluon's colour partner is now the colour partner of the original quark, and its anticolour partner the quark, and the colour partner of the quark is the gluon. One of the partons will radiate with the maximum angle given by the direction of the new colour partner and so on until the cut-off is reached, of order 1 GeV, below which emission does not occur. This procedure then resums both the leading soft and collinear singularities.

In processes where there is more than one Feynman diagram it is possible for the colour flows in the diagrams to be different. This leads to so called "non-planar" terms from the interference terms, where the colour flows do not match. These are not positive definite and hence cannot be interpreted in a probabilistic way for implementation in the Monte Carlo procedure. They are always suppressed by inverse powers of N_c. A procedure must be adopted to split up the "non-planar" parts of the tree-level matrix element to give redefined planar terms with positive-definite coefficients that can be used in the Monte Carlo procedure. Such a procedure was proposed in [21] and shown to work correctly for all QCD processes. However, as shown in [27], this is inadequate for MSSM processes and hence a new procedure was proposed, which we adopt here. In this procedure the "non-planar" parts of the matrix element are split up according to

$$|\overline{M}|^2_{\mathrm{full},i} = \frac{|\overline{M}|^2_i}{|\overline{M}|^2_{\mathrm{planar}}} |\overline{M}|^2_{\mathrm{tot}} \,, \tag{2.10}$$

where $|\overline{M}|^2_i$ is the matrix element squared for the ith colour flow, $|\overline{M}|^2_{\mathrm{planar}}$ is the sum of the matrix elements squared for the planar colour flows, and $|\overline{M}|^2_{\mathrm{tot}}$ is the total matrix element squared. This ensures that the terms are positive definite and the new full planar terms have the correct pole structure and sum to the correct total cross section. This can then be implemented numerically.

In this section we have explained how by using a Markov branching procedure we can resum both the soft and collinear singularities in QCD.

2.3 Hadronization

After the parton shower phase it is necessary to adopt some procedure to combine the quarks and gluons into the observed hadrons. This is done in the HERWIG event generator using the *cluster hadronization model* [28]. This model is based on the concept of colour preconfinement. This implies that the invariant mass of pairs of colour-connected partons has a spectrum that is peaked at low values, a few times the cut off used in the parton-shower, and is universal, i.e. independent of the hard scale and type of the collision, as discussed below and shown in figure $11a$.

In the cluster hadronization model [28], after the end of the parton showering process we are left with gluons and quarks. The gluons are non-perturbatively split into light quark-antiquark pairs. The final state then consists only of quarks and antiquarks which are, in the planar approximation, uniquely paired in colour-anticolour pairs. These pairs of colour-connected quarks do not necessarily have the correct invariant mass to form a meson. Instead they are formed into colour-singlet meson-like resonance called "clusters". These clusters then decay in their rest frame to a pair of hadrons (either two mesons or a baryon and an antibaryon) with the type of hadron determined by the available phase space. In the original model of [28] these decays were isotropic in the rest frame of the cluster, however in the current implementation of the model [17], the hadrons containing the quarks from the perturbative stage of the event continue in the same direction (in the cluster rest frame) as the original quark.

It is reasonable to assume that the low-mass clusters are superpositions of hadron resonances and can be treated in this way [28]. However, a fraction of the clusters have higher masses for which this assumption is not valid and these clusters are first split using a string-like mechanism [28] into lighter clusters before they are decayed to hadrons.

A simple extension of this model is used for hadron remnants. For example in a collision in which a valence quark from a proton participates in a hard process, the two remaining valence quarks are left in the final state. They are paired up as a 'diquark' which, in the planar approximation, carries an anticolour index and can be treated like an antiquark. The resulting cluster has baryonic quantum numbers and decays into a baryon and a meson.

3. Angular ordering in $\not{R}_{\rm p}$

In Standard Model and MSSM processes apart from complications involving processes where there are "non-planar" terms [27] the angular ordering procedure is relatively straightforward to implement. However in $\not{R}_{\rm p}$ SUSY there are additional complications.

The lepton number violating processes, which come from the first two terms in the superpotential, eq. (1.2), have colour flows that are the same as those which occur in the MSSM. On the other hand, the baryon number violating interactions, which come from the third term in eq. (1.2), have a very different colour structure involving the totally antisymmetric tensor, $\epsilon^{c_1c_2c_3}$. We look first at the colour structure of the various baryon number violating decays which we include in the Monte Carlo simulation and then at the structure of the various hard scattering processes.

3.1 Decays

From the point of view of the colour structure there are three types of baryon number violating decays which we include in the Monte Carlo simulation.

1. Two-body $\not{B}$ decay of an antisquark to two quarks or a squark to two antiquarks.
2. Three-body $\not{B}$ decay of a colourless sparticle, i.e. a neutralino or a chargino, to three quarks or antiquarks.
3. Three-body $\not{B}$ decay of the gluino to three quarks or antiquarks.

In general it is possible to consider for example the decay of a neutralino to three quarks as either a three-body decay or two sequential two-body decays, of the neutralino to an antisquark and a quark and then of the antisquark to two quarks. If either of the two sequential two-body decays are kinematically forbidden, i.e. they can only proceed if the internal particle in the three-body decay is off-shell, then we consider the decay to be three-body, otherwise we treat the decay as two sequential two-body decays.

The problem is then how to implement the angular ordering procedure for these three processes. We shall consider them using the eikonal current with an arbitrary number of colours as was done in section 2.2.1 for the process $e^+e^- \to q\bar{q}g$. So in these R-parity violating processes this means we need to consider the decay of an antisquark to (N_c-1) quarks and of the neutralino, chargino and gluino to N_c quarks. We also have to use the generalization to N_c colours of the antisymmetric tensor, i.e. $\epsilon^{c_1\ldots c_{N_c}}$.

3.1.1 Squark decays

For the decay of an antisquark to (N_c-1) quarks the leading infrared contribution to the soft gluon distribution has the following factorized form:

$$\mathbf{M}(p_0,p_1,p_2,\ldots,p_{N_c-1};q) = g_s\mathbf{m}(p_0,p_1,p_2,\ldots,p_{N_c-1})\cdot\mathbf{J}(q)\,, \tag{3.1}$$

where

- $\mathbf{m}(p_0,p_1,p_2,\ldots,p_{N_c-1})$ is the tree-level matrix element for an antisquark, with momentum p_0, to decay to N_c-1 quarks, with momentum $p_1,\ldots,p_{N_c-1}$.

- $\mathbf{M}(p_0, p_1, p_2, \ldots, p_{N_c-1}; q)$ is the tree-level matrix element for the decay of an antisquark to $N_c - 1$ quarks including the emission of an extra soft gluon, with momentum q.

- $\mathbf{J}(q)$ is the non-abelian semi-classical current for the emission of the soft gluon with momentum q from the hard partons.

- c_0 is the colour of the decaying antisquark and $c_1, \ldots, c_{N_c-1}$ are the colours of the quarks.

Again the current, $\mathbf{J}(q)$, is given by, $\mathbf{J}(q) = \sum_{s=1,2} \mathbf{J}^{b,\mu}(q)\varepsilon_{\mu,s}$ where here

$$\mathbf{J}^{b,\mu}(q) = -\left(\frac{p_0^\mu}{p_0 \cdot q}\right) \mathbf{t}^{b,\tilde{q}^*}_{c_0,c_0'} \epsilon^{c_0',c_1,\ldots,c_{N_c-1}} + \sum_{i=1}^{N_c-1} \left(\frac{p_i^\mu}{p_i \cdot q}\right) \mathbf{t}^{b,q_i}_{c_i,c_i'} \epsilon^{c_0,\ldots,c_i',\ldots,c_{N_c-1}} . \tag{3.2}$$

b and μ are the colour and Lorentz indices of the emitted gluon; $\mathbf{t}^{b,\tilde{q}^*}$, $\mathbf{t}^{b,q_i}$ are the colour matrices of the antisquark and quarks, respectively.

We obtain the soft gluon distribution simply by squaring the current

$$\mathbf{J}^2(q) = -C_F N_c (N_c - 2)! \left[\sum_{i=1}^{N_c-1} \left(\frac{p_0}{p_0 \cdot q} - \frac{p_i}{p_i \cdot q} \right)^2 + \sum_{i=1}^{N_c-1} \sum_{j>i}^{N_c-1} \left(\frac{p_i}{p_i \cdot q} - \frac{p_j}{p_j \cdot q} \right)^2 \right] . \tag{3.3}$$

This can be expressed in terms of the radiation functions as in eq. (2.5), where here the tree-level colour factor is $C_{\mathbf{m}} = \epsilon^{c_0,\ldots,c_{N_c-1}} \epsilon^{c_0,\ldots,c_{N_c-1}} = N_c!$ where we have not averaged over the initial colours, and the radiation pattern is given by

$$W(\Omega_q) = \frac{-\omega^2 C_F}{(N_c - 1)} \left[\sum_{i=1}^{N_c-1} \left(\frac{p_0}{p_0 \cdot q} - \frac{p_i}{p_i \cdot q} \right)^2 + \sum_{i=1}^{N_c-2} \sum_{j>i}^{N_c-1} \left(\frac{p_i}{p_i \cdot q} - \frac{p_j}{p_j \cdot q} \right)^2 \right] . \tag{3.4}$$

We can then re-express this result in terms of the functions given in [22]

$$W(\Omega_q) = \frac{2 C_F}{(N_c - 1)} \sum_{i=0}^{N_c-1} \sum_{j \neq i}^{N_c-1} W_{ij}^i . \tag{3.5}$$

This is exactly the same result obtained in [29], in the context of baryon number violation in the Standard Model, except that the massless radiation functions of their paper are now replaced by the massive functions here.

This leads to the following approach for treating the soft gluon radiation from this process. The quarks from the decay are randomly colour connected to either the decaying antisquark or the other quark. This then correctly treats the soft gluon radiation from the decay products. It should be noted that this is only the colour connection for the angular ordering procedure. This colour connection for the hadronization of these events is discussed in section 4.

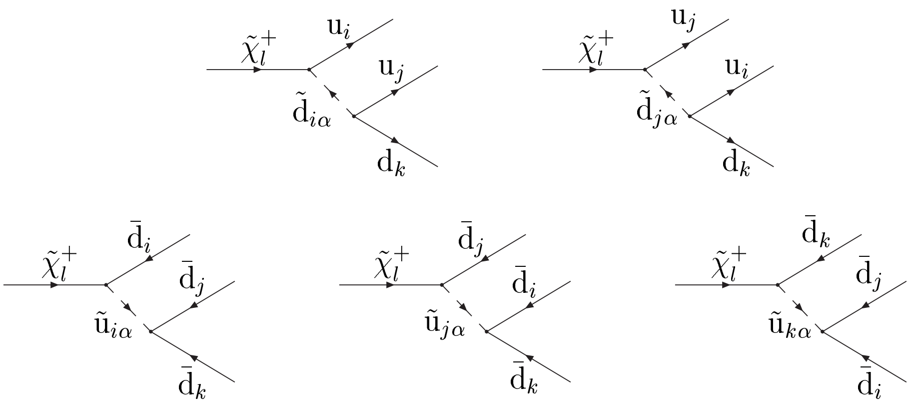

Figure 3: UDD decays of the $\tilde{\chi}^+$.

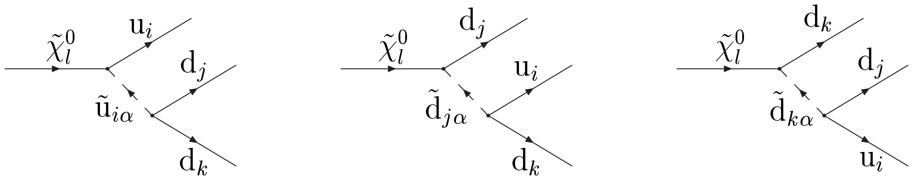

Figure 4: UDD decays of the $\tilde{\chi}^0$.

In general, the QCD radiation from sparticles, which are here in the *initial* state, is neglected in HERWIG. We would expect this approximation to be valid for two reasons, firstly the sparticles will usually have a short lifetime and secondly, due to their heavy masses the QCD radiation will also be suppressed unless they have momenta much greater than their masses. However for the decays we consider, we can include the effects of radiation from the decaying sparticles. This is done by treating the radiation in the rest frame of the decaying squark where there is no radiation from the decaying sparticle, which HERWIG would not generate anyway. However as stated in section 2.2.1 while the radiation from individual partons, i.e. W^i_{ij}, is not Lorentz invariant the dipole radiation functions are. Hence the total radiation pattern is Lorentz invariant and therefore by treating the decay in the rest frame of the decaying particle we correctly include the QCD radiation from the decaying particle when we boost back to the lab frame.

3.1.2 Chargino and neutralino decays

The charginos decay via the process shown in figure 3, and the neutralinos via the process in figure 4. If we consider the QCD radiation from the decay of a colour neutral object which decays, for an arbitrary number of colours N_c, to N_c quarks, then we see that there is only one possible colour flow for this process. The squarks appearing in these processes, $\tilde{q}_{i\alpha}$, can be either of the states $\alpha = 1, 2$ resulting from

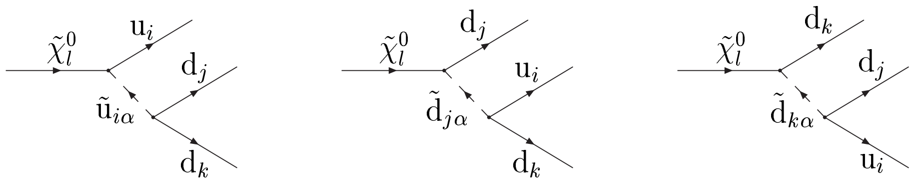

Figure 5: UDD decays of the $\tilde{\mathrm{g}}$.

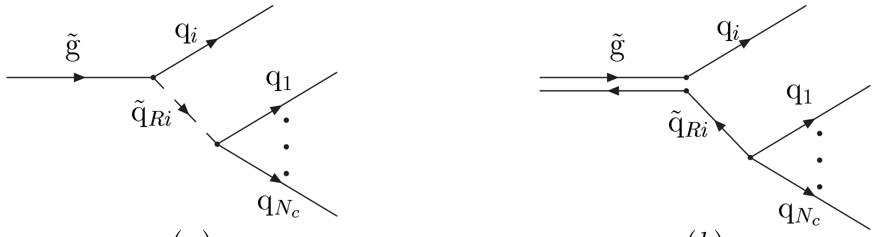

(a) (b)

Figure 6: Baryon number violating decay of $\tilde{g}$. (a) Feynman diagram. (b) Colour flow.

the mixing of $\tilde{\mathrm{q}}_{iL}$ and $\tilde{\mathrm{q}}_{iR}$, as discussed in more detail in the appendix. In fact, the colour structure of this process is very similar to that of the squark decay and the matrix element in the soft limit can be written in the same factorized form as before. Again, we can express the current as in eq. (2.5) where the tree-level colour factor $C_{\mathbf{m}} = \epsilon^{c_0,\ldots,c_{N_c-1}}\epsilon^{c_0,\ldots,c_{N_c-1}} = N_c!$ and the radiation function is given by

$$W(\Omega_q) = \frac{2C_F}{(N_c-1)} \sum_{i=1}^{N_c} \sum_{j\neq i}^{N_c} W^i_{ij}\,. \tag{3.6}$$

This result can be interpreted as saying that a quark in the final state should be randomly connected to any of the other quarks from the neutralino or chargino decays. Again this is only the colour connection for the angular ordering procedure, the colour connections for the hadronization phase are discussed in section 4.

3.1.3 Gluino decays

The colour structure of the gluino decay is very different from that of the colourless objects or the squarks which we have already considered, the diagrams for this process are shown in figure 5. Again if we consider an arbitrary number of colours, N_c, the gluino will decay to N_c quarks. In this case there will be N_c possible colour flows, corresponding to the Feynman diagrams and colour flows shown in figure 6. These different colour flows will lead to "non-planar" terms which must be dealt with.

The leading infrared contribution to the soft gluon distribution can be written in the following factorized form:

$$\mathbf{M}(p_0,p_1,p_2,\ldots,p_{N_c};q) = g_s \sum_{i=1}^{N_c} \mathbf{m}_i(p_0,p_1,p_2,\ldots,p_{N_c}) \cdot \mathbf{J}_i(q)\,, \tag{3.7}$$

where

- $\mathbf{m}_i(p_0, p_1, p_2, \ldots, p_{N_c})$ is the tree-level matrix element of the three-body gluino decay for the i-th possible colour flow.
- $\mathbf{M}(p_0, p_1, p_2, \ldots, p_{N_c}; q)$ is the tree-level matrix element for the three-body gluino decay including the extra emission of a soft gluon of momentum q.
- $\mathbf{J}_i(q)$ is the non-abelian semi-classical current for the emission of the soft gluon, momentum q, from the hard partons for the i-th possible colour flow.

Again the current has the form $\mathbf{J}_i(q) = \sum_{s=1,2} \mathbf{J}_i^{b,\mu}(q)\varepsilon_{\mu,s}$, where in this case

$$\mathbf{J}_i^{b,\mu}(q) = i\left(\frac{p_0^\mu}{p_0 \cdot q}\right)\mathbf{f}^{ba'a}\mathbf{t}^{a'}_{c_i c'_i}\epsilon^{c_1\ldots c'_i\ldots c_{N_c}} + \left(\frac{p_i^\mu}{p_i \cdot q}\right)\mathbf{t}^{b}_{c_i c'_i}\mathbf{t}^{a}_{c'_i c''_i}\epsilon^{c_1\ldots c''_i\ldots c_{N_c}} + \\ + \sum_{j=1,j\neq i}^{N_c}\left(\frac{p_j^\mu}{p_j \cdot q}\right)\mathbf{t}^{b}_{c_j c'_j}\mathbf{t}^{a}_{c_i c'_i}\epsilon^{c_1\ldots c'_i\ldots c'_j\ldots c_{N_c}}\,. \tag{3.8}$$

We can write the matrix element squared for this process as

$$|\mathbf{M}(p_0, p_1, p_2, \ldots, p_{N_c}; q)|^2 = g_s^2\sum_{i=1}^{N_c}|\mathbf{m}_i(p_0, p_1, p_2, \ldots, p_{N_c})|^2 \cdot |\mathbf{J}_i(q)|^2 + \\ + g_s^2\sum_{i=1}^{N_c}\sum_{j=1,j\neq i}^{N_c}\mathbf{m}_i\mathbf{m}_j^* \cdot \mathbf{J}_i(q)\cdot\mathbf{J}_j^*(q)\,. \tag{3.9}$$

The procedure of [27], which was described in section 2 can be used with the matrix elements for this process given in appendix to deal with the "non-planar" terms. So we now consider the radiation pattern of the planar terms. The current can be written as in eq. (2.5) where here the tree-level colour factor

$$C_{\mathbf{m}} = \mathbf{t}^{b}_{c_i c'_i}\epsilon^{c_1\ldots c'_i\ldots c_{N_c}}\mathbf{t}^{b}_{c''_i c_i}\epsilon^{c_0\ldots c''_i\ldots c_{N_c}} = C_F N_c!\,. \tag{3.10}$$

We have not averaged over the initial colours, and the radiation function is given by

$$W(\Omega_q) = C_A W^0_{0i} + 2C_F W^i_{0i} + \frac{2C_F}{(N_c-1)}\sum_{j\neq i,k\neq i,j}^{N_c} W^j_{jk} + \\ + \frac{1}{(N_c-1)}\sum_{j\neq i}^{N_c}\left(C_A W^0_{0j} + 2C_F W^j_{0j}\right) + \\ + \frac{1}{N_c}W^i_{0i} + \frac{1}{N_c(N_c-1)}\sum_{j\neq i}^{N_c}\left(W^j_{0j} - W^i_{ij} - W^j_{ij}\right). \tag{3.11}$$

This planar piece of the soft radiation pattern gives us the result we would naïvely expect. This pattern can be thought of as saying the i-th quark should be connected

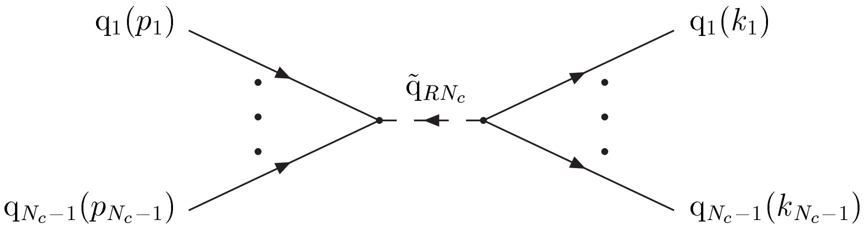

Figure 7: Resonant squark production followed by $\not{B}$ decay for an arbitrary number of colours N_c.

to the colour line of the gluino as in an MSSM process and the anti-colour line of the gluino and the remaining quarks should be randomly connected in the same way as for the baryon number violating squark decay. This radiation pattern, eq. (3.11), also contains pieces which are of order $1/N_c^2$ with respect to the leading order pieces that we will neglect as in section 2. We therefore connect the i-th quark to the gluino in the standard MSSM way with probability given by $\frac{|M|^2_{\mathrm{full},i}}{|M|^2_{\mathrm{tot}}}$, where $|M|^2_{\mathrm{full},i}$ is given by eq. (2.10). We can then treat the anti-colour line and the remaining quarks as a decaying antisquark.

3.2 Hard processes

In addition to the decays which we have already discussed, there are a number of baryon number violating hard subprocesses we include in the simulation. All of the colour structures of the hard processes that actually violate baryon number have already been discussed as these processes are merely crossed versions of the various decays discussed above. However in addition to these processes there are some hard processes that occur via the third term in the superpotential but involve no net baryon number violation, e.g. figure 7.

We will therefore only discuss this type of process which cannot be obtained by crossing the previous results.

3.2.1 Resonant squark production followed by $\not{B}$ decay

As before, we will consider the process in figure 7 for an arbitrary number of colours, N_c.

We can write the matrix element for the emission of an extra soft gluon in the following form:

$$\mathbf{M}(p_1, \ldots, p_{N_c-1} : k_1, \ldots, k_{N_c-1}; q) = g_s \mathbf{m}(p_1, \ldots, p_{N_c-1} : k_1, \ldots, k_{N_c-1}) \cdot \mathbf{J}(q)\,, \tag{3.12}$$

where

- $\mathbf{m}(p_1, \ldots, p_{N_c-1} : k_1, \ldots, k_{N_c-1})$ is the tree-level matrix element for the $(N_c - 1)$ quarks to $(N_c - 1)$ quarks scattering.

- $\mathbf{M}(p_1, \ldots, p_{N_c-1} : k_1, \ldots, k_{N_c-1}; q)$ is the tree-level matrix element for the $(N_c - 1)$ quarks to $(N_c - 1)$ quarks scattering with the additional emission of a soft gluon with momentum q.

- $\mathbf{J}(q)$ is the non-abelian semi-classical current for the emission of the soft gluon, momentum q, from the hard partons.

- $p_1, \ldots, p_{N_c-1}$ are the momenta of the partons in the initial state.

- $k_1, \ldots, k_{N_c-1}$ are the momenta of the partons in the final state.

Again the current has the form $\mathbf{J}(q) = \sum_{s=1,2} \mathbf{J}^{b,\mu}(q)\varepsilon_{\mu,s}$, where in this case

$$\begin{aligned} \mathbf{J}^{b,\mu}(q) = &- \sum_{i=1}^{N_c-1} \left(\frac{p_i^\mu}{p_i \cdot q} \right) \mathbf{t}^b_{c'_i c_i} \epsilon^{c_1 \ldots c'_i \ldots c_{N_c}} \epsilon^{d_1 \ldots d_{N_c-1} c_{N_c}} + \\ &+ \sum_{i=1}^{N_c-1} \left(\frac{k_i^\mu}{k_i \cdot q} \right) \mathbf{t}^b_{d_i d'_i} \epsilon^{c_1 \ldots c_{N_c-1} d_{N_c}} \epsilon^{d_1 \ldots d'_i \ldots d_{N_c}} , \end{aligned} \tag{3.13}$$

where b and μ are the colour and Lorentz indices of the emitted gluon, respectively.

We can now obtain the soft gluon distribution by squaring the current. This can be rewritten using eq. (2.5) where here the tree-level colour factor is given by $C_{\mathbf{m}} = N_c!(N_c - 1)!$, again we have not averaged over the initial state colours, and the radiation function is given by

$$\begin{aligned} W(\Omega_q) = &\frac{2C_F}{(N_c - 1)} \sum_{i=1}^{N_c-1} \sum_{j \neq i} W^i_{ij} + \frac{2C_F}{(N_c - 1)} \sum_{l=1}^{N_c-1} \sum_{m \neq l} W^l_{lm} + \\ &+ \frac{2C_F}{(N_c - 1)^2} \sum_{i=1}^{N_c-1} \sum_{l=1}^{N_c-1} \left(W^i_{il} + W^l_{il} \right) , \end{aligned} \tag{3.14}$$

where the partons i and j are in the initial state and the partons l and m are in the final state.

This radiation pattern gives quite an unusual angular ordering procedure. If we consider one of the quarks in the initial state, this quark should be randomly connected to any of the other quarks in the initial state or to the final state, i.e. the probability of connecting to a given quark in the initial state and the final state as a whole is equal. If the quark is connected to the final state it must then be connected at random to one of the final state quarks. Similarly the final state quarks are connected at random to any of the other final state quarks or the initial state, and again quarks connected to the initial state are then randomly connected to any of the initial state quarks.

4. Hadronization in $\not{R}_p$

As we saw in section 3, it is possible to angular order the baryon number violating decays and hard processes. It is then necessary to decide how to hadronize these events using the cluster hadronization model [28] for a full simulation of these processes. The procedure described in section 2 also works in the MSSM provided that the lifetime of the coloured sparticles does not exceed the hadronization time-scale. However some modifications to this model are required for $\not{R}_p$ processes.

In the Standard Model and MSSM cases the colour partner for the colour coherence effects and for the hadronization phase are always the same. In the $\not{B}$ decays and hard processes we see for the first time cases where the colour connection for the angular ordering and for the hadronization can be different. This is because while the colour connection for the angular ordering procedure is determined by the eikonal current, the colour connection for the hadronization phase is defined by the colour flow in the leading order diagram. When baryon number is conserved these are identical, however when baryon number is violated, there are cases where the two are different.

First we consider the simplest type of decay, i.e. a neutralino or chargino decaying to three quarks. The method described in section 3 correctly implements the angular ordering procedure. After the parton-shower phase (and the splitting of remaining gluons to quark anti-quark pairs) we will be left with pairs of colour connected partons forming colour singlets as well as *three* further quarks. An example of this is shown in figure 8. These three remaining quarks form a colour singlet with baryonic quantum numbers, a baryonic cluster. To handle baryonic clusters HERWIG needs the constituents to be labelled as one quark and one diquark rather than three quarks, so we randomly pair two of them up as a diquark. In our example in figure 8 the three quarks in the middle together form a colour singlet which is combined into a baryon.

This procedure is relatively easy to implement in the case of electroweak gaugino decays. However it becomes more difficult in the case of the $\not{B}$ decay of a squark to two quarks. If the colour partner of the decaying squark is a particle which decays via a baryon number conserving process then the two quarks and the particle which gets the colour of the second decaying particle can be clustered as in the neutralino case, e.g. in figure 9 the u_i, d_j, d_k should be formed into a baryonic cluster.

However, if this second particle decays via $\not{B}$ as well, then the procedure must be different, as shown in figure 10. Here, instead of forming one baryonic cluster, we form two mesonic clusters. This is done by pairing the d_k randomly with either the $\bar{\mathrm{d}}_l$ or $\bar{\mathrm{d}}_m$ into a standard colour singlet, the remaining quark and antiquark are also paired into a colour singlet. This is not the colour connection for the angular ordering but the colour connection for the hadronization phase, which is different in this case and determined by the colour flow in the tree-level diagram.

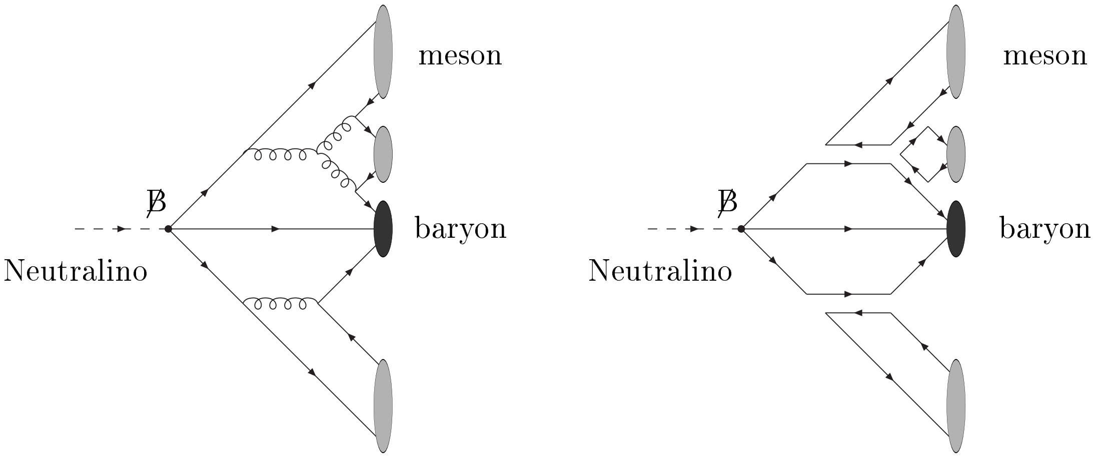

Figure 8: The Feynman diagrams and colour flows for the hadronization of a $\not B$ neutralino decay.

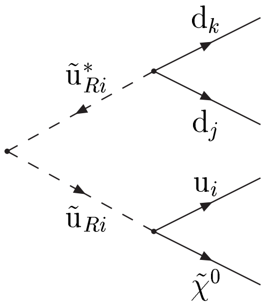

Figure 9: Hadronization with one $\not B$ decay.

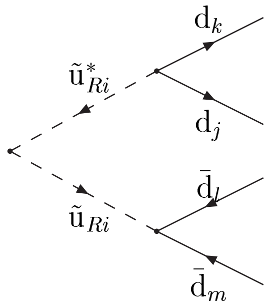

Figure 10: Hadronization with two $\not B$ decays.

This leaves the case of the gluino decay for which it is easiest to consider the two colour lines separately. The colour line should be treated as normal and the anticolour line like a decaying antisquark. So if the anticolour partner of the gluino is a Standard Model particle or decays via a baryon number conserving MSSM decay mode we form the three quarks into a baryonic cluster. However if the anticolour partner decays via a $\not B$ mode we then form two mesonic clusters.

There is one further type of colour flow to be considered which is the production of a resonant squark via $\not B$ which then also decays via $\not B$. The correct hadronization procedure in this case is similar to that adopted for the case of two colour connected $\not B$ decays. We randomly connect the final state quarks to the colour partners of either of the initial state quarks to form a colour singlet. The remaining final state quark can then be paired with the colour partner of the other initial state quark. This gives two colour-singlet clusters. Again the colour partner for hadronization is determined by the colour flow in the tree-level diagram. Using the procedures we have outlined above it is possible to hadronize any of the $\not B$ decays or hard processes.

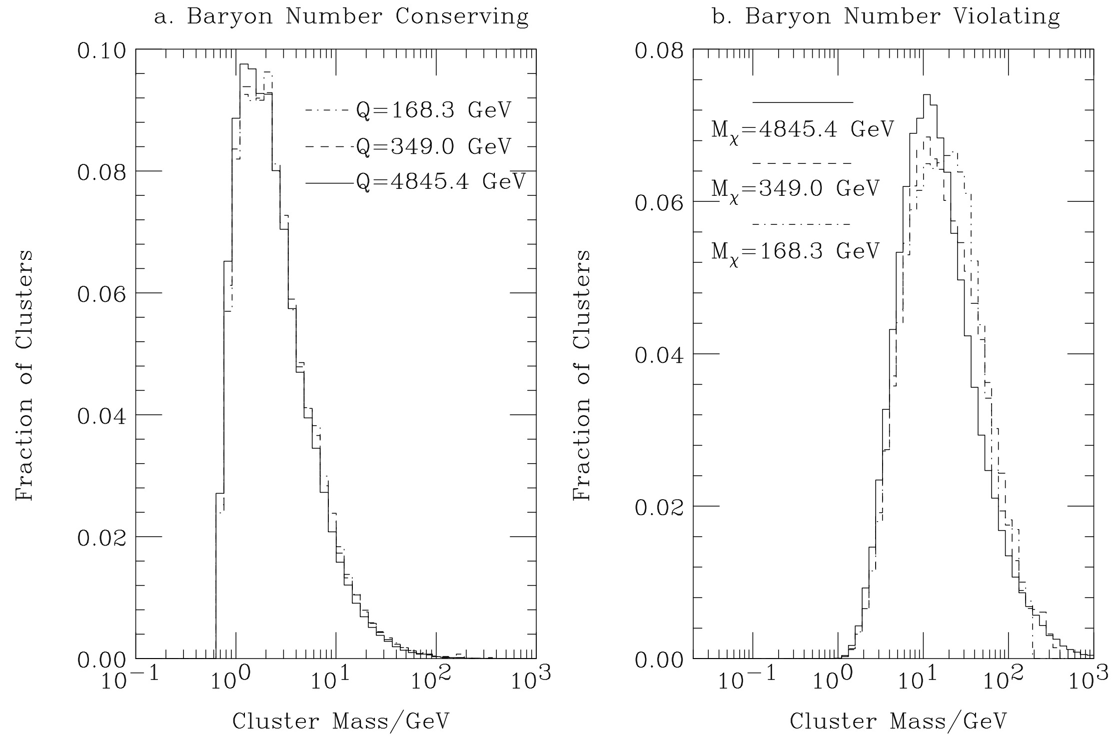

Figure 11: Distributions of the colour singlet cluster masses. The baryon number conserving clusters come from e^+e^- events at the given scale whereas the baryon number violating clusters come from decays of neutralinos at the given masses.

There is however one potential problem. The cluster model is based on the idea of colour preconfinement. In baryon number violating processes we see a very different spectrum for the baryonic clusters formed from the baryon number violation to that seen for clusters in the hitherto studied Standard Model events. Figure 11 shows the spectra for both Standard Model and baryon number violating clusters. The spectrum for the baryon number violating clusters peaks at a much higher mass than the baryon number conserving clusters and has a large tail at high masses. This therefore means that before these clusters are decayed to hadrons most of them must be split into lighter clusters. The spectrum of the baryon number conserving clusters in these events has the same spectrum as in Standard Model events.

Figure 11 contains the mass spectrum of pairs of colour connected partons after the parton-shower phase and the non-perturbative splitting of the gluons into quark-antiquark pairs. The baryon number conserving clusters, figure 11a, contains all the clusters in e^+e^- events at the given centre-of-mass energies, whereas the baryon number violating clusters, figure 11b only contains those clusters which contain the three quarks left after all the other quarks are paired into colour-singlets from neutralino decays at the given mass.

The joining clusters in figure 12a shows the clusters from e^+e^- events with one quark from the parton-shower of the quark, and an antiquark from the parton-shower

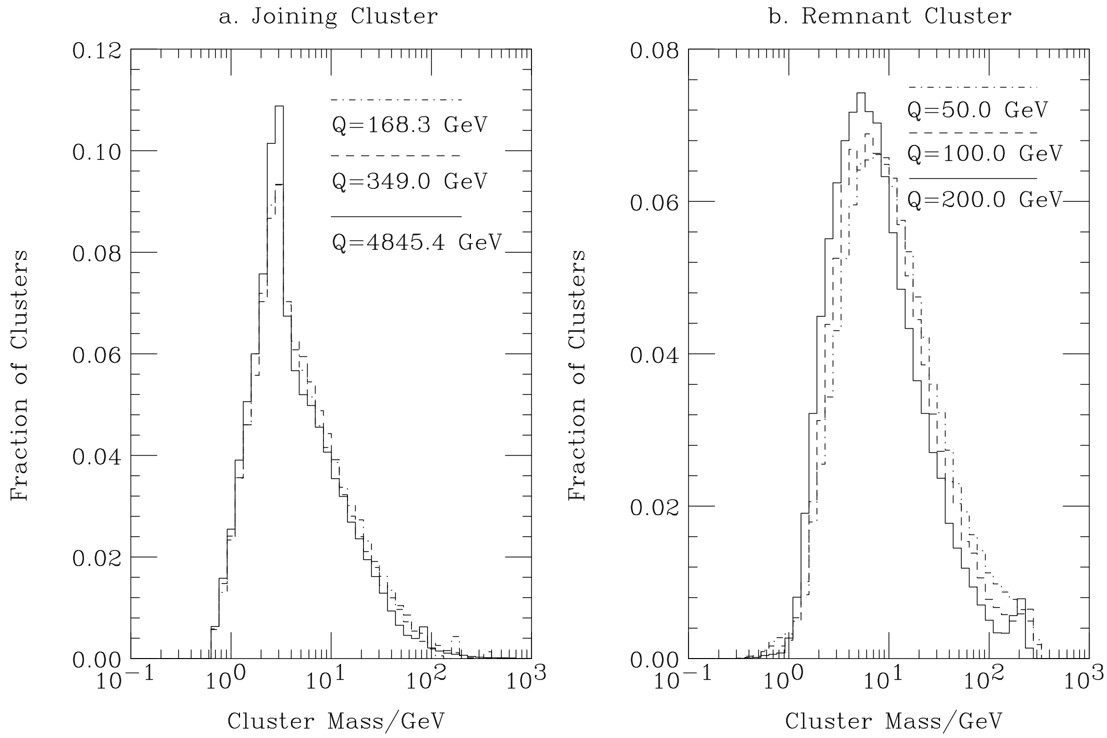

Figure 12: Masses of the joining and remnant clusters. The joining clusters are from e^+e^- events at the given scale. The remnant clusters were generated in e^-p events with 30 GeV electrons and 820 GeV protons with the given scale as the minimum value of Q.

JHEP04(2000)008

of the antiquark. The remnant clusters, figure 12*b* come from the cluster in DIS events which contains the diquark, formed from two of the valence quarks.

We would expect the baryon-number violating clusters to be heavier than the standard baryon number conserving clusters because

1. The baryonic cluster is formed from three quarks originating from three *different* jets, as also shown in figure 11 of the neutralino decay. In normal $e^+e^- \to$ hadrons events the clusters joining partons from different jets are heavier than the clusters which come entirely from partons from one jet, figure 12*a*;

2. The new cluster contains a diquark and in general the clusters containing diquarks in for example the hadron remnant in deep inelastic scattering are heavier than the normal quark-antiquark clusters, figure 12*b*.

As these clusters are heavier they will be more sensitive to the fine details of the hadronization model. In particular these clusters are sensitive to the maximum cluster mass before the clusters are split and the details of this splitting mechanism. It is worth noting that the same is true of the joining clusters in $e^+e^- \to 3$ jet events, and it is precisely these clusters that contribute to the "string effect", which is well described by HERWIG.

5. Preliminary results

We have implemented the R-parity violating decays and hard processes into the HERWIG Monte Carlo event generator according to the algorithms given in sections 3 and 4. They are available in the latest version 6.1 [17]. Having taken care to implement colour coherence effects, it is of immediate interest to see whether they have a significant influence on observable final-state distributions. To this end we have studied some jet production processes and compared the final-state distributions with those from standard QCD two-jet events. It was observed in ref. [25] that certain variables can be constructed that are particularly sensitive to colour coherence effects. In particular these variables are sensitive to the presence of colour connections that link the initial and final states. To investigate these effects for the different colour connection structures of the $\not{R}_{\mathrm{p}}$ models, we will study these variables for two-jet production via resonant sparticle production in hadron-hadron collisions. We essentially follow the details of the analysis of ref. [25].

As examples we study the processes

- $\bar{\mathrm{u}}\mathrm{d} \to \bar{\mathrm{u}}\mathrm{d}$ via a resonant stau, and $\bar{\mathrm{d}}\mathrm{d} \to \bar{\mathrm{d}}\mathrm{d}$ via a resonant tau sneutrino, this occurs via the coupling λ'_{311}. The Feynman diagrams for this process are shown in figure 13. This process involves lepton-number violating couplings but no baryon number violating vertices.

- Resonant squark production via the coupling λ''_{212}. This leads to resonant down, strange and charm squark production. The resonant diagram for this process is shown in figure 7.

These couplings were chosen to try and maximize the cross section given the experimental constraints on the couplings. The coupling λ'_{311} has an upper bound, at the 2σ level, given by [11]

$$\lambda'_{311} < 0.11 \left(\frac{M_{\tilde{\mathrm{d}}_R}}{100\,\mathrm{GeV}} \right). \tag{5.1}$$

While the bounds on other LQD couplings are weaker they involve higher generation quarks and hence the cross sections will be suppressed by the parton luminosities.

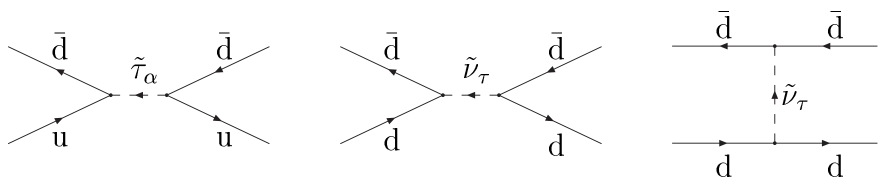

Figure 13: Feynman diagrams for $\bar{\mathrm{u}}\mathrm{d} \to \bar{\mathrm{u}}\mathrm{d}$ and $\bar{\mathrm{d}}\mathrm{d} \to \bar{\mathrm{d}}\mathrm{d}$.

Similarly for the resonant squark production the couplings that couple two first-generation quarks would in principle give the highest cross sections. However, the limits on these couplings are so strict that we used λ''_{212}, which is only limited by perturbativity [11].

We would expect very different results for the variables that are sensitive to the initial-final state colour connections for these two processes. The first process only has such colour connection in the relatively suppressed t-channel sneutrino diagram, whereas the second process has initial-final state colour connections in the resonant diagram due to the random colour structure at the $\not{B}$ vertex. This is the effect we wish to demonstrate explicitly below.

5.1 Resonant slepton production

For resonant slepton production we consider both the signal and the background which were generated using the program described in ref. [17]. The only cut made was to require the presence of at least one jet with E_T of greater than 200 GeV in the event. A parton level cut requiring the p_T of the two final-state partons to be greater than 150 GeV each, was used to reduce the number of events we needed to simulate, however this should not affect the results. The signal points were generated using the following SUGRA parameters, $M_0 = 600\,\mathrm{GeV}$, $M_{\frac{1}{2}} = 200\,\mathrm{GeV}$, $A_0 = 0\,\mathrm{GeV}$, $\tan\beta = 10$, and $\mathrm{sgn}\mu = +$. At this SUGRA point the right down squark mass is 728 GeV which corresponds to a limit of $\lambda'_{311} < 0.80$. The third generation lepton masses are all close to 600 GeV, $M_{\tilde{\tau}_1} = 599$ GeV, $M_{\tilde{\tau}_2} = 617$ GeV, $M_{\tilde{\nu}_\tau} = 610$ GeV. These processes have previously been considered in [30, 15].

The results in all the graphs correspond to the number of events at Run II of the Tevatron, with centre of mass energy of 2 TeV, and integrated luminosity of $2\mathrm{fb}^{-1}$.

As can been seen in figure 14, the results for two different values of the coupling show that there is a bump in the di-jet invariant mass distribution, M_{jj}, from the resonant particle production for large values of the coupling.

We can now study the events around the bump, $580\,\mathrm{GeV} \leq M_{jj} \leq 640\,\mathrm{GeV}$, in the distribution and plot the variables that are sensitive to angular ordering for these events [25]. These variables depend on the distribution of a third jet in the events which is generated in the simulation by the parton-shower algorithm. The three relevant variables are: η_3, R and α. They are defined in the following way: (1) If we define the jets in the order of their E_T, with jet 1 being the hardest jet in the event, then η_3 is the pseudo-rapidity of the third jet. (2) Defining $\Delta\eta \equiv \eta_3 - \eta_2$ and the difference in polar angles $\Delta\phi \equiv \phi_3 - \phi_2$, then the variable $R \equiv \sqrt{\Delta\eta^2 + \Delta\phi^2}$. This is the distance between the second and third jets in the (η, ϕ) space. (3) If we first define $\Delta H \equiv \mathrm{sgn}(\eta_2)\Delta\eta$, we can then consider the polar angle in the $(|\Delta\phi|, \Delta H)$ space. This is $\alpha \equiv \tan^{-1}(\Delta H/|\Delta\phi|)$.

In the analysis in ref. [25] additional cuts were imposed in terms of these new variables, which we also implement in our analysis.

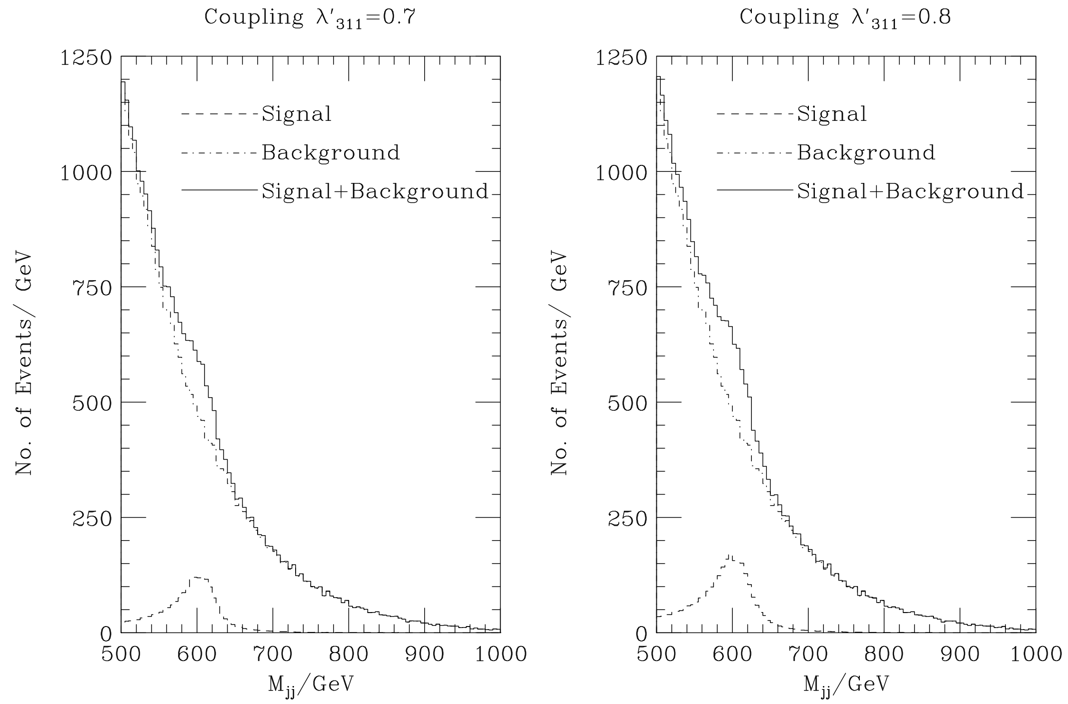

Figure 14: Di-jet invariant mass distribution for $\lambda'_{311} = 0.7$ and $\lambda'_{311} = 0.8$.

1. A pseudo-rapidity cut on the two highest p_T jets in the event, $|\eta_1|, |\eta_2| < 0.7$.
2. Requiring the two leading jets in E_T to be back to back $||\phi_1 - \phi_2| - \pi| < 20°$.
3. We require the transverse energy of the third jet, $E_{T3} > 10\,\text{GeV}$ to avoid background from the underlying event.
4. For the study of α only, we make the additional cut $1.1 < R < \pi$ to avoid problems with overlapping cones in the jet clustering algorithm.

We can now study the distributions for the signal, the background and the signal plus background for the resonant slepton production with coupling $\lambda'_{311} = 0.8$. There are significant differences between the signal and the background for this process. In the η_3 distributions, figure 15, instead of a dip in the background at $\eta_3 = 0$ there is a bump in the signal. This dip in the QCD background was observed in [25], and is a feature of the initial-final state colour connection. In our study it is present in the background, but not the signal.

The distribution of events in R, shown in figure 16, is very similar for both the signal and background. In fact in the study of [25] all the event generators, even those which do not include angular ordering, gave good agreement with the data for this observable. The distribution of events in α, figure 17, also shows a difference between the signal and the background, with the signal not showing the dip in the middle. This is again an effect of the initial-final state colour connection which is present in the background but not in the signal.

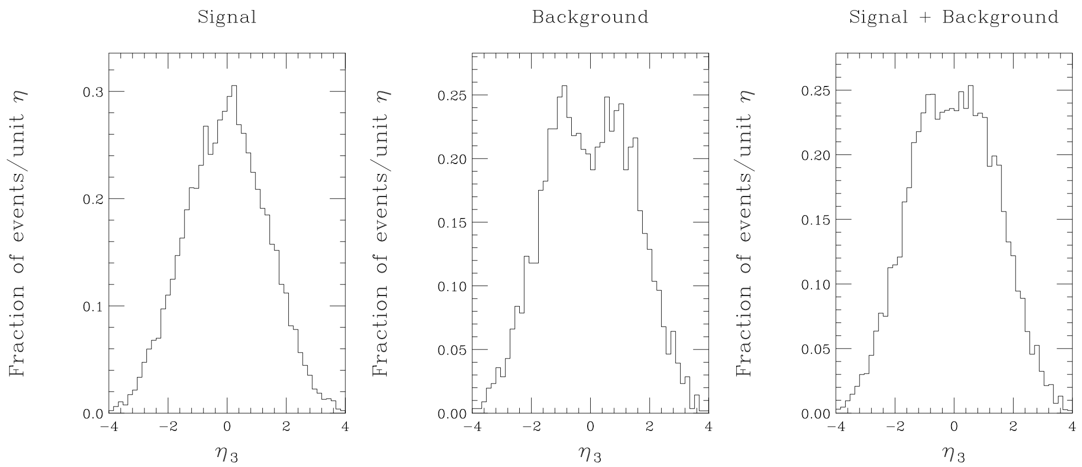

Figure 15: The distribution of events in η_3 for (a) the resonant slepton production, (b) the QCD background, and (c) the combination of the two.

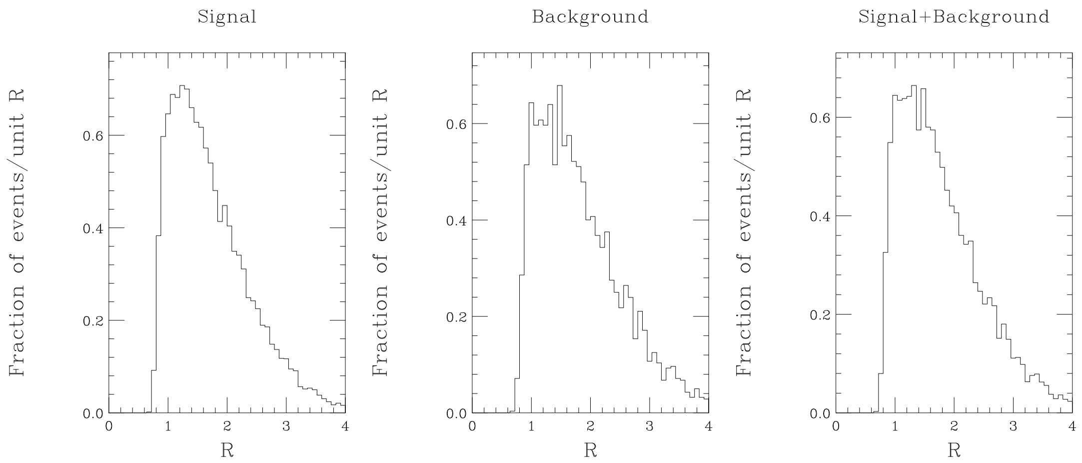

Figure 16: The distribution of events in R for (a) the resonant slepton production, (b) the QCD background, and (c) the combination of the two.

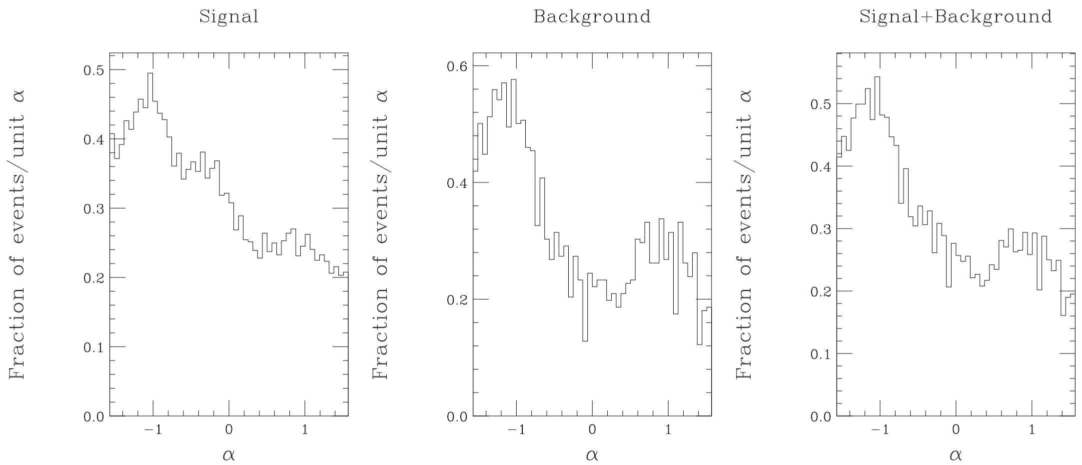

Figure 17: The distribution of events in α for (a) the resonant slepton production, (b) the QCD background and (c) the combined events.

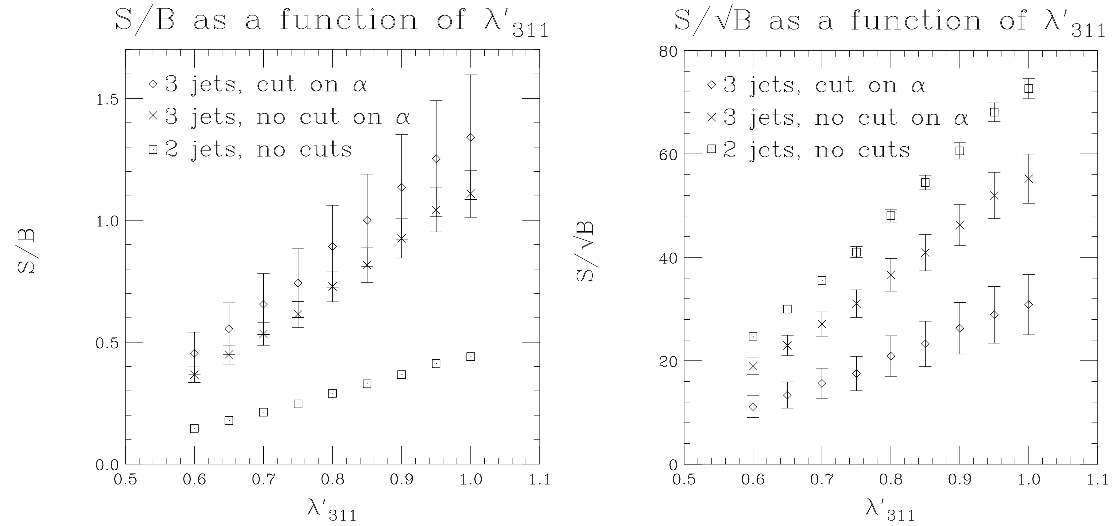

Figure 18: Effect of the cuts on the angular ordering variables as a function of λ'_{311}.

As can be seen in all the distributions apart from the disappearance of the dip at $\eta_3 = 0$, once the signal and background are added the effect of the signal is minimal. While there are differences between the signal and background it is hard to see how cuts can be applied on these variables to improve the extraction of a signal over the QCD background. The only major difference which can be cut on is the difference in the distribution of α. We consider two approaches to increase the ratio of signal to background S/B.

1. Accept all the events with at least three jets, provided they pass the cuts described above from the analysis of [25].

2. Reject all the two jet events and only accept the events with more than two jets provided that $|\alpha| \leq \alpha_{\text{cut}}$. We apply a cut of $\alpha_{\text{cut}} = 0.4$ for these jet events.

These cuts were chosen to maximize S/B while not reducing $S/\sqrt{B}$ below five. As can be seen in figure 18 both of these cuts significantly increase the S/B. This can be seen in the effect on the invariant mass distribution with the second cut, figure 19. In the invariant mass distribution the signal is now more visible over the background.

This shows that by using the colour coherence effects we can improve the extraction of a signal. We would expect obtaining a large S/B to be important for this process because we do not have an accurate prediction for the QCD background. However given the limits on this coupling this signal will only be visible above the background at the highest couplings currently allowed by low-energy experiments. In [30, 15] it was suggested that by using the sidebands to normalize the background that resonant slepton production could be probed to much smaller values of the couplings. Indeed the $S/\sqrt{B}$ numbers in figure 18 suggest that without any of our additional cuts the signal is visible at much lower couplings. However their results

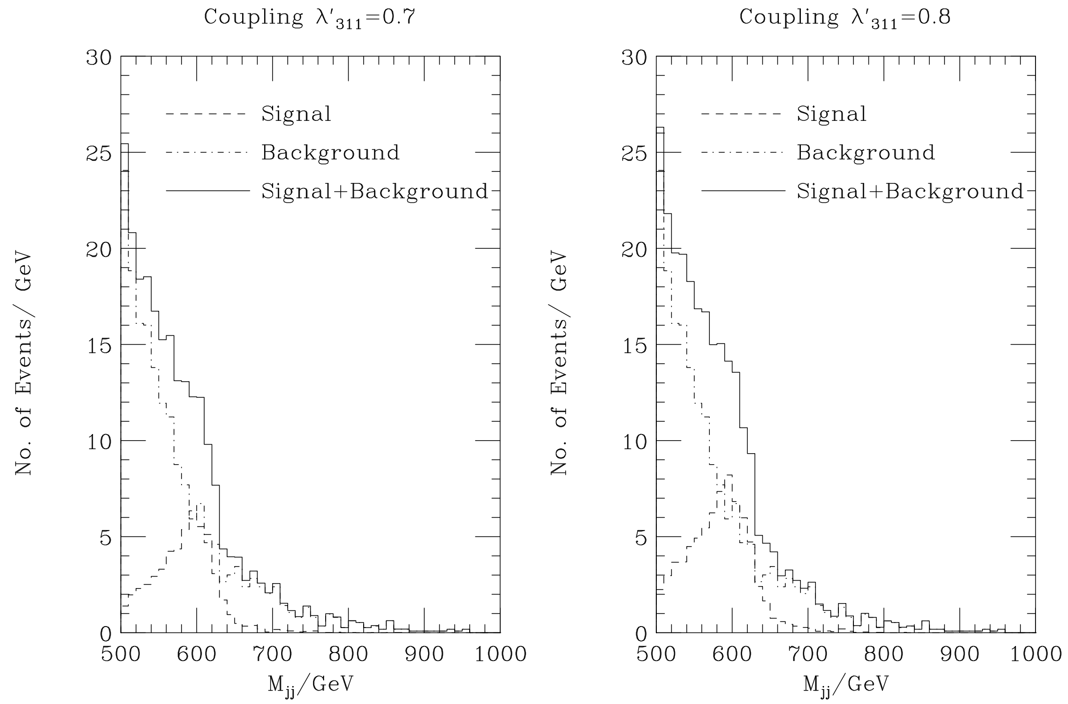

Figure 19: Invariant mass distribution for $\lambda'_{311} = 0.7$ and $\lambda'_{311} = 0.8$ after cuts on the angular ordering variables.

were obtained using the narrow-width limit for the production cross section and did not included the effects of QCD radiation. Our results suggest that after including these effects the signal will only be visible for large values of the coupling. It may be possible to use the sidebands which we have removed with our cuts to normalize this background, as in [30, 15], to improve the extraction of the signal. However this may not be possible due to the increased width of the resonance, figure 14, due to QCD radiation. The situation will hopefully improve with the availability of a next-to-leading order calculation for the QCD background. At present if we require a reasonable S/B ratio of 25% in addition to $S/\sqrt{B} > 5$, then simply looking at the di-jet invariant masses will only allow couplings of $\lambda'_{311} > 0.75$ to be probed. However using the cuts suggested based on the colour structure couplings as low as $\lambda'_{311} > 0.55$ can be probed.

5.2 Resonant squark production

The cross section at the Tevatron for resonant squark production[2] is much lower than the resonant slepton production due to the reduced parton luminosity.

(This will be reversed at the LHC.) It is therefore unlikely that an excess of events can be seen over the QCD background. It is however still interesting to look at the distributions of the angular ordering variables. The signal point was generated using

[2]Resonant squark production via $U_i D_j D_k$ has previously been considered in [31].

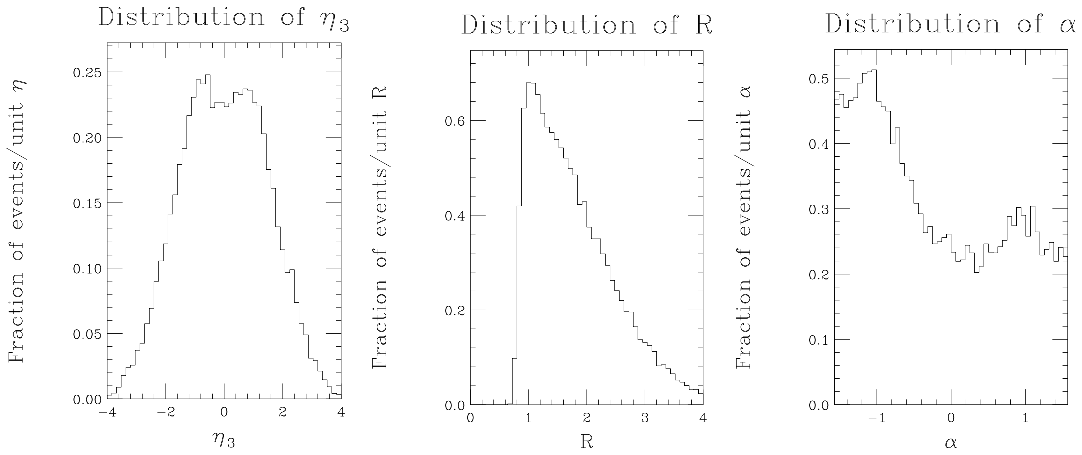

Figure 20: Distributions of the signal for resonant squark production.

the following SUGRA parameters, $M_0 = 500\,\text{GeV}$, $M_{\frac{1}{2}} = 200\,\text{GeV}$, $A_0 = 0\,\text{GeV}$, $\tan\beta = 10$, and $\text{sgn}\mu = +$ and $\lambda''_{212} = 1$. At this point the squark mass $M_{\tilde{\text{d}}_R,\tilde{\text{s}}_R,\tilde{\text{c}}_R} =$ 601 GeV. As can be seen in figure 20, there is now less difference in the shape of the distribution between the signal and the background (c.f. figures 15, 16, 17). The resonant squark production shows a dip at $\eta_3 = 0$ and a rise as $\alpha \to \pi/2$, which is due to the colour connection between the initial and final states. The effect is slightly less than for the QCD background as there are combinatorially fewer such connections.

The fact that the final state distributions of the resonant slepton and resonant squark production processes are so different, despite the identities and kinematics of the jets themselves being so similar, clearly shows that colour coherence plays an important role in determining the properties of R-parity violating processes. Even if this is not used as a tool to enhance the signal, it is likely that it will affect the efficiency of any cuts that are applied, so it is essential that any experiments looking for R-parity violating processes take into account colour coherence in their simulations of the signal.

Even if R-parity violating hard processes were added to ISAJET [16], it would not be expected to describe the final state well, as it is based on the incoherent parton shower and independent fragmentation models. Thus, in our case for example, the resonant slepton and resonant squark processes would have very similar properties. It is worth noting that ISAJET gives a poor description of the CDF data [25] on η_3, R and α in standard QCD two-jet events.

6. Conclusion

We have presented a procedure for implementing colour coherence effects via the angular ordering procedure in R-parity violating SUSY models. We find that the baryon number violating processes have a random colour connection structure for angular ordering. In these processes we see for the first time differences in the colour partners for the colour coherence effects and those used with the idea of colour preconfinement for hadronization in the cluster model.

A full set of decays and hadron-hadron cross sections have now been implemented in the HERWIG Monte Carlo event generator [17, 18]. The first preliminary results for these processes show that the inclusion of colour coherence is important and that for some processes we can use the colour coherence properties of the processes to help extract an R-parity violating SUSY signature.

The availability of a full simulation should allow a more detailed experimental study of these processes for the first time.

Acknowledgments

P. Richardson would like to thank PPARC for a research studentship, number PPA/S/S/1997/02517. We thank P. Gondolo for helpful discussions.

A. Conventions

Here we present all the matrix elements for R-parity violating two- and three-body decays of sparticles as well as the matrix elements for single sparticle production via $2 \to 2$ scattering processes. We disregard those possibilities where the sfermion resonance kinematically is not probed, e.g.

$$d_j + \bar{d}_k \to \tilde{\nu}_i \to \tilde{\nu}_i + Z^0 \,. \tag{A.1}$$

We also do not consider the processes generated from quark-photon scattering as discussed in [32]. First we present the decay matrix elements of the sfermions, neutralinos, charginos and the gluino. We will then give the matrix elements for the cross sections most of which can simply be obtained by crossing the various decay matrix elements. Throughout we allow for more than one $\not{R}_{\mathrm{p}}$ coupling to be non zero.

We follow the conventions of [33, 34] for the neutralino and chargino mixing matrices and the convention of [35] for the mixing of the sfermions. For the current eigenstates $\tilde{q}^i_{L,R}$ and the mass eigenstates $\tilde{q}^i_{1,2}$ the mixing is

$$\begin{pmatrix} \tilde{q}^i_L \\ \tilde{q}^i_R \end{pmatrix} = \begin{pmatrix} \cos\theta^i_q & \sin\theta^i_q \\ -\sin\theta^i_q & \sin\theta^i_q \end{pmatrix} \begin{pmatrix} \tilde{q}^i_1 \\ \tilde{q}^i_2 \end{pmatrix} . \tag{A.2}$$

We denote the mixing matrix above as Q^i_{jk} where $i = u,\, d,\, s,\, c,\, b,\, t$ is the quark flavour index. The analogous slepton mixing matrix is denoted L^i_{jk}, where $i = \mathrm{e}^-,\, \nu_{\mathrm{e}},\, \mu^-,\, \nu_\mu,\, \tau^-,\, \nu_\tau$ is the lepton flavour index. We neglect inter-generational sfermion mixing. As we do not consider the right-handed neutrino we also neglect the lepton mixing. We give the formulae below for general generation indices. However, in HERWIG, the mixing for the first two generations of sleptons and squarks is not included as it is expected to be small.

In order to simplify the notation for the matrix elements we introduce the following functions:

$$\begin{aligned} R(\tilde{a}, m^2_{bc}) &\equiv \frac{1}{(m^2_{bc} - M^2_{\tilde{a}})^2 + \Gamma^2_{\tilde{a}} M^2_{\tilde{a}}}\,, && \text{(A.3)} \\ S(\tilde{a}, \tilde{b}, m^2_{cd}, m^2_{ef}) &\equiv R(\tilde{a}, m^2_{cd}) R(\tilde{b}, m^2_{ef}) \times \\ &\quad \times \Big[(m^2_{cd} - M^2_{\tilde{a}})(m^2_{ef} - M^2_{\tilde{b}}) + \Gamma_{\tilde{a}}\Gamma_{\tilde{b}} M_{\tilde{a}} M_{\tilde{b}} \Big]. && \text{(A.4)} \end{aligned}$$

Here $m^2_{bc} = (p_b + p_c)^2$, and $M_{\tilde{a}}$, $\Gamma_{\tilde{a}}$ are the mass and the decay width of the sfermion $\tilde{a}$, respectively. The various terms in the matrix elements can be more easily expressed in terms of

$$\begin{aligned} \Psi(\tilde{a}, 1, 2, 3) &\equiv R(\tilde{a}, m^2_{12}) \left(m^2_{12} - m^2_1 - m^2_2 \right) \times \\ &\quad \times \Big[\left(a^2(\tilde{a}) + b^2(\tilde{a}) \right) \left(M^2_0 + m^2_3 - m^2_{12} \right) + 4a(\tilde{a}) b(\tilde{a}) m_3 M_0 \Big], && \text{(A.5)} \\ \Upsilon(\tilde{a}, 1, 2, 3) &\equiv S(\tilde{a}_1, \tilde{a}_2, m^2_{12}, m^2_{12}) \left(m^2_{12} - m^2_1 - m^2_2 \right) \times \\ &\quad \times \Big[\left(a(\tilde{a}_1) a(\tilde{a}_2) + b(\tilde{a}_1) b(\tilde{a}_2) \right) \left(M^2_0 + m^2_3 - m^2_{12} \right) + \\ &\qquad + 2 \left(a(\tilde{a}_1) b(\tilde{a}_2) + a(\tilde{a}_2) b(\tilde{a}_1) \right) m_3 M_0 \Big], && \text{(A.6)} \\ \Phi(\tilde{a}, \tilde{b}, 1, 2, 3) &\equiv S(\tilde{a}, \tilde{b}, m^2_{12}, m^2_{23}) \times \\ &\quad \times \Big[m_1 m_3 a(\tilde{a}) a(\tilde{b}) \left(m^2_{12} + m^2_{23} - m^2_1 - m^2_3 \right) + \\ &\qquad + m_1 M_0 b(\tilde{a}) a(\tilde{b}) \left(m^2_{23} - m^2_2 - m^2_3 \right) + \\ &\qquad + m_3 M_0 a(\tilde{a}) b(\tilde{b}) \left(m^2_{12} - m^2_1 - m^2_2 \right) + \\ &\qquad + b(\tilde{a}) b(\tilde{b}) \left(m^2_{12} m^2_{23} - m^2_1 m^2_3 - M^2_0 m^2_2 \right) \Big]. && \text{(A.7)} \end{aligned}$$

Here $\tilde{a}_1$ and $\tilde{a}_2$ are the mass eigenstates of the relevant SUSY particle. The functions a and b are gaugino-sfermion-fermion coupling constants and are given in the tables below: table 2 for the neutralino, table 3 for the chargino and table 4 for the gluino. The couplings are defined such that $a(\tilde{c}^*) = b(\tilde{c})$, and $b(\tilde{c}^*) = a(\tilde{c})$. In all the above expressions M_0 is the mass of the decaying sparticle and 1, 2 and 3, are the decay products.

B. Decays

B.1 Sfermions

Here we present the matrix elements for the two-body sfermion decays including left/right mixing. In general the spin and colour averaged matrix elements have

JHEP04(2000)008

Operator	Process	Colour factor and coupling C^a_{bc}
LLE	$\tilde{e}^-_{j\alpha} \to \bar{\nu}_i \ell^-_k$	$\lvert\lambda_{ijk}\rvert^2 \lvert L^{2j-1}_{1\alpha}\rvert^2$
LLE	$\tilde{e}^-_{k\alpha} \to \nu_i \ell^-_j$	$\lvert\lambda_{ijk}\rvert^2 \lvert L^{2k-1}_{2\alpha}\rvert^2$
LLE	$\tilde{\nu}_j \to \ell^+_i \ell^-_k$	$\lvert\lambda_{ijk}\rvert^2$
LQD	$\tilde{e}^-_{i\alpha} \to \bar{u}_j d_k$	$N_c \lvert\lambda'_{ijk}\rvert^2 \lvert L^{2i-1}_{1\alpha}\rvert^2$
LQD	$\tilde{\nu}_i \to \bar{d}_j d_k$	$N_c \lvert\lambda'_{ijk}\rvert^2$
LQD	$\tilde{d}_{j\alpha} \to \bar{\nu}_i d_k$	$\lvert\lambda'_{ijk}\rvert^2 \lvert Q^{2j-1}_{1\alpha}\rvert^2$
LQD	$\tilde{u}_{j\alpha} \to e^+_i d_k$	$\lvert\lambda'_{ijk}\rvert^2 \lvert Q^{2j}_{1\alpha}\rvert^2$
LQD	$\tilde{d}_{k\alpha} \to \nu_i d_j$	$\lvert\lambda'_{ijk}\rvert^2 \lvert Q^{2k-1}_{2\alpha}\rvert^2$
LQD	$\tilde{d}_{k\alpha} \to e^-_i u_j$	$\lvert\lambda'_{ijk}\rvert^2 \lvert Q^{2k-1}_{2\alpha}\rvert^2$
UDD	$\tilde{u}_{i\alpha} \to \bar{d}_j \bar{d}_k$	$(N_c-1)! \lvert\lambda''_{ijk}\rvert^2 \lvert Q^{2i}_{2\alpha}\rvert^2$
UDD	$\tilde{d}_{k\alpha} \to \bar{u}_i \bar{d}_j$	$(N_c-1)! \lvert\lambda''_{ijk}\rvert^2 \lvert Q^{2k-1}_{2\alpha}\rvert^2$

Table 1: Coefficients for the scalar decays.

the form

$$|\overline{\mathbf{M}}(a \to b, c)|^2 = C^a_{bc}(M_a^2 - m_b^2 - m_c^2)\,, \tag{B.1}$$

where C^a_{bc} is the colour factor and the coupling for the process. These factors are tabulated for the various sfermion decays in table 1. N_c denotes the number of colours.

In all these terms the Roman indices represent the generation of the particle and the Greek indices the mass eigenstate of the sfermions when there is mixing. The decay rate can be obtained by integrating over the two-body phase space. This gives

$$\Gamma(a \to b, c) = \frac{|\overline{\mathbf{M}}(a \to b, c)|^2 p_{cm}}{8\pi M_a^2}\,, \tag{B.2}$$

where p_{cm} is the final-state momentum in the rest frame of the decaying particle

$$p_{cm}^2 = \frac{1}{4M_a^2}\left[M_a^2 - (m_b + m_c)^2\right]\left[M_a^2 - (m_b - m_c)^2\right]. \tag{B.3}$$

B.2 Neutralinos

The total three-body decay rate of a photino was first computed in [36] in the limit where the sfermion is much heavier than the decaying photino and assuming massless final states. In [37] the general photino matrix element squared was given, allowing for the computation of final-state distributions. In [38, 39] this was extended

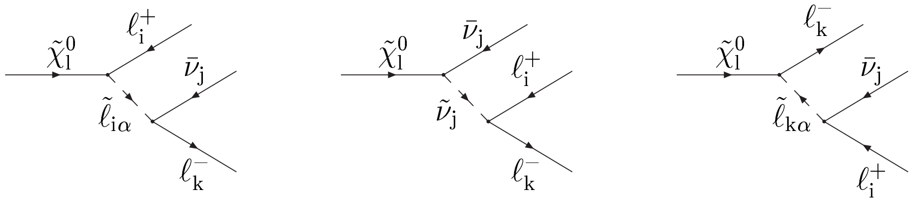

Figure 21: LLE decays of the $\tilde{\chi}$.

to the general case of a neutralino. In [39] arbitrary sfermion mixing was included as well. We have recalculated the rates with only left/right sfermion mixing (neglecting intergenerational sfermion mixing). We use a different convention both for the $R\!\!\!/_{\rm p}$ superpotential and the MSSM lagrangean, which is more appropriate to the implementation in HERWIG. The LLE, LQD and UDD decay modes are shown in figures 21, 22, 4, respectively.

There are four decay modes:

1. $\tilde{\chi}^0 \to \bar{\nu}_{\rm i}\ell^+_{\rm j}\ell^-_{\rm k}$,
2. $\tilde{\chi}^0 \to \bar{\nu}_{\rm i}\bar{\rm d}_{\rm j}{\rm d}_{\rm k}$,
3. $\tilde{\chi}^0 \to \ell^+_{\rm i}\bar{\rm u}_{\rm j}{\rm d}_{\rm k}$,
4. $\tilde{\chi}^0 \to \bar{\rm u}_{\rm i}\bar{\rm d}_{\rm j}\bar{\rm d}_{\rm k}$,

as well as their complex conjugates, since the neutralino is a Majorana fermion. The spin and colour averaged matrix elements are given below.[3]

$$
\begin{aligned}
&|\,\overline{\mathbf{M}}(\,\tilde{\chi}^0_l \to \bar{\nu}_i\ell^+_j\ell^-_k\,)\,|^2 = \\
&= \lambda^2_{ijk}\Big[\Psi(\tilde{\nu}_i,\ell_j,\ell_k,\nu_i) + \sum_{\alpha=1,2}|L^{2j-1}_{1\alpha}|^2\Psi(\tilde{\ell}_{j\alpha},\nu_i,\ell_k,\ell_j) + \\
&\qquad + \sum_{\alpha=1,2}|L^{2k-1}_{2\alpha}|^2\Psi(\tilde{\ell}^*_{k\alpha},\nu_i,\ell_j,\ell_k) + \\
&\qquad + 2L^{2j-1}_{11}L^{2j-1}_{12}\Upsilon(\tilde{\ell}_j,\nu_i,\ell_k,\ell_j) + 2L^{2k-1}_{21}L^{2k-1}_{22}\Upsilon(\tilde{\ell}^*_k,\nu_i,\ell_j,\ell_k) - \\
&\qquad - \sum_{\alpha=1,2}2L^{2j-1}_{1\alpha}\Phi(\tilde{\ell}_{j\alpha},\tilde{\nu}_i,\nu_i,\ell_k,\ell_j) - \sum_{\alpha=1,2}2L^{2k-1}_{2\alpha}\Phi(\tilde{\ell}^*_{k\alpha},\tilde{\nu}_i,\nu_i,\ell_j,\ell_k) - \\
&\qquad - \sum_{\alpha=1,2}\sum_{\beta=1,2}2L^{2j-1}_{1\alpha}L^{2k-1}_{2\beta}\Phi(\tilde{\ell}^*_{k\beta},\tilde{\ell}_{j\alpha},\ell_j,\nu_i,\ell_k)\Big]\,,
\end{aligned}
\tag{B.4}
$$

[3] We have a slight disagreement with [39] concerning the sign of the width of the sfermions. This is numerically insignificant since when the sfermion is on-shell HERWIG treats this as a two-body decay. The authors of [39] agree with our signs. We thank Paolo Gondolo for discussion of this point.

$$
\begin{aligned}
&|\overline{\mathbf{M}}(\,\tilde\chi^0_l \to \bar\nu_i \bar d_j d_k\,)|^2 = \\
&= \lambda'^2_{ijk} N_c \Big[\Psi(\tilde\nu_i, d_j, d_k, \nu_i) + \sum_{\alpha=1,2} |Q^{2j-1}_{1\alpha}|^2 \Psi(\tilde d_{j\alpha}, \nu_i, d_k, d_j) + \\
&\qquad + \sum_{\alpha=1,2} |Q^{2k-1}_{2\alpha}|^2 \Psi(\tilde d^*_{k\alpha}, \nu_i, d_j, d_k) + \\
&\qquad +2Q^{2j-1}_{11} Q^{2j-1}_{12} \Upsilon(\tilde d_j, \nu_i, d_k, d_j) + 2Q^{2k-1}_{21} Q^{2k-1}_{22} \Upsilon(\tilde d^*_k, \nu_i, d_j, d_k) - \\
&\qquad - \sum_{\alpha=1,2} 2Q^{2j-1}_{1\alpha} \Phi(\tilde d_{j\alpha}, \tilde\nu_i, \nu_i, d_k, d_j) - \sum_{\alpha=1,2} 2Q^{2k-1}_{2\alpha} \Phi(\tilde d^*_{k\alpha}, \tilde\nu_i, \nu_i, d_j, d_k) - \\
&\qquad - \sum_{\alpha=1,2} \sum_{\beta=1,2} 2Q^{2j-1}_{1\alpha} Q^{2k-1}_{2\beta} \Phi(\tilde d^*_{k\beta}, \tilde d_{j\alpha}, d_j, \nu_i, d_k) \Big], \qquad \text{(B.5)}
\end{aligned}
$$

$$
\begin{aligned}
&|\overline{\mathbf{M}}(\,\tilde\chi^0_l \to \ell^+_i \bar u_j d_k\,)|^2 = \\
&= \lambda'^2_{ijk} N_c \left[\sum_{\alpha=1,2} |L^{2i-1}_{1\alpha}|^2 \Psi(\tilde\ell_{i\alpha}, u_j, d_k, \ell_i) + \sum_{\alpha=1,2} |Q^{2j}_{1\alpha}|^2 \Psi(\tilde u_{j\alpha}, \ell_i, d_k, u_j) + \right. \\
&\qquad + \sum_{\alpha=1,2} |Q^{2k-1}_{2\alpha}|^2 \Psi(\tilde d^*_{k\alpha}, \ell_i, u_j, d_k) + 2L^{2i-1}_{11} L^{2i-1}_{12} \Upsilon(\tilde\ell_i, u_j, d_k, \ell_i) + \\
&\qquad +2Q^{2j}_{11} Q^{2j}_{12} \Upsilon(\tilde u_j, \ell_i, d_k, u_j) + 2Q^{2k-1}_{21} Q^{2k-1}_{22} \Upsilon(\tilde d^*_k, \ell_i, u_j, d_k) - \\
&\qquad - \sum_{\alpha=1,2} \sum_{\beta=1,2} 2L^{2i-1}_{1\alpha} Q^{2j}_{1\beta} \Phi(\tilde u_{j\beta}, \tilde\ell_{i\alpha}, \ell_i, d_k, u_j) - \\
&\qquad - \sum_{\alpha=1,2} \sum_{\beta=1,2} 2L^{2i-1}_{1\alpha} Q^{2k-1}_{2\beta} \Phi(\tilde d^*_{k\beta}, \tilde\ell_{i\alpha}, \ell_i, u_j, d_k) - \\
&\qquad \left. - \sum_{\alpha=1,2} \sum_{\beta=1,2} 2Q^{2j}_{1\alpha} Q^{2k-1}_{2\beta} \Phi(\tilde d^*_{k\beta}, \tilde u_{j\alpha}, u_j, \ell_i, d_k) \right], \qquad \text{(B.6)}
\end{aligned}
$$

$$
\begin{aligned}
&|\overline{\mathbf{M}}(\,\tilde\chi^0_l \to \bar u_i \bar d_j \bar d_k\,)|^2 = \\
&= \lambda''^2_{ijk} N_c! \left[\sum_{\alpha=1,2} |Q^{2i}_{2\alpha}|^2 \Psi(\tilde u^*_{i\alpha}, d_j, d_k, u_i) + \sum_{\alpha=1,2} |Q^{2j-1}_{2\alpha}|^2 \Psi(\tilde d^*_{j\alpha}, u_i, d_k, d_j) + \right. \\
&\qquad + \sum_{\alpha=1,2} |Q^{2k-1}_{2\alpha}|^2 \Psi(\tilde d^*_{k\alpha}, u_i, d_j, d_k) + 2Q^{2i}_{21} Q^{2i}_{22} \Upsilon(\tilde u^*_i, d_j, d_k, u_i) + \\
&\qquad +2Q^{2j-1}_{21} Q^{2j-1}_{22} \Upsilon(\tilde d^*_j, u_i, d_k, d_j) + 2Q^{2k-1}_{21} Q^{2k-1}_{22} \Upsilon(\tilde d^*_k, u_i, d_j, d_k) - \\
&\qquad - \sum_{\alpha=1,2} \sum_{\beta=1,2} 2Q^{2i-1}_{2\alpha} Q^{2j-1}_{2\beta} \Phi(\tilde d^*_{j\beta}, \tilde u^*_{i\alpha}, u_i, d_k, d_j) - \\
&\qquad - \sum_{\alpha=1,2} \sum_{\beta=1,2} 2Q^{2i-1}_{2\alpha} Q^{2k-1}_{2\beta} \Phi(\tilde d^*_{k\beta}, \tilde u^*_{i\alpha}, u_i, d_j, d_k) - \\
&\qquad \left. - \sum_{\alpha=1,2} \sum_{\beta=1,2} 2Q^{2j-1}_{2\alpha} Q^{2k-1}_{2\beta} \Phi\Big(\tilde d^*_{k\beta}, \tilde d^*_{j\alpha}, d_j, u_i, d_k\Big) \right]. \qquad \text{(B.7)}
\end{aligned}
$$

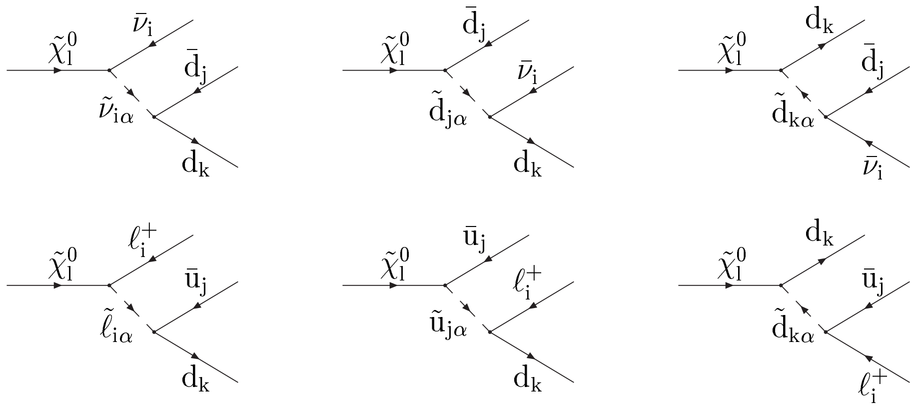

Figure 22: LQD decays of the $\tilde{\chi}$.

Coefficient	
$a(\tilde{\nu}_i)$	0
$b(\tilde{\nu}_i)$	$\frac{gN'_{l2}}{2\cos\theta_w}$
$a(\tilde{\ell}_{i\alpha})$	$m_{\ell_i}\frac{gN_{l3}}{2M_W\cos\beta}L^{2i-1}_{1\alpha}+L^{2i-1}_{2\alpha}\left(eN'_{l1}-\frac{g\sin^2\theta_w N'_{l2}}{\cos\theta_w}\right)$
$b(\tilde{\ell}_{i\alpha})$	$m_{\ell_i}\frac{gN_{l3}}{2M_W\cos\beta}L^{2i-1}_{2\alpha}-L^{2i-1}_{1\alpha}\left(eN'_{l1}+\frac{gN'_{l2}\left(1/2\ -\sin^2\theta_w\right)}{\cos\theta_w}\right)$
$a(\tilde{d}_{i\alpha})$	$m_{d_i}\frac{gN_{l3}}{2M_W\cos\beta}Q^{2i-1}_{1\alpha}-Q^{2i-1}_{2\alpha}\left(ee_dN'_{l1}-\frac{ge_d\sin^2\theta_w N'_{l2}}{\cos\theta_w}\right)$
$b(\tilde{d}_{i\alpha})$	$m_{d_i}\frac{gN_{l3}}{2M_W\cos\beta}Q^{2i-1}_{2\alpha}+Q^{2i-1}_{1\alpha}\left(ee_dN'_{l1}-\frac{gN'_{l2}\left(1/2\ +e_d\sin^2\theta_w\right)}{\cos\theta_w}\right)$
$a(\tilde{u}_{i\alpha})$	$m_{u_j}\frac{gN_{l4}}{2M_W\sin\beta}Q^{2j}_{1\alpha}-Q^{2j}_{2\alpha}\left(ee_uN'_{l1}-\frac{ge_u\sin^2\theta_w N'_{l2}}{\cos\theta_w}\right)$
$b(\tilde{u}_{i\alpha})$	$m_{u_i}\frac{gN_{l4}}{2M_W\sin\beta}Q^{2i}_{2\alpha}+Q^{2i}_{1\alpha}\left(ee_uN'_{l1}+\frac{gN'_{l2}\left(1/2\ -e_u\sin^2\theta_w\right)}{\cos\theta_w}\right)$

Table 2: Couplings for the neutralino decays.

When the neutralino mass matrix is diagonalized it is possible to get negative eigenvalues in which case the physical field is $\gamma_5\chi$ rather than χ. This then changes the sign of some of the coefficients in table 2: the coefficients $a(\tilde{c})$ change sign, and hence the coefficients $b(\tilde{c}^*)$ also change sign.

The partial widths can be obtained from these matrix elements by integrating over any two of m^2_{12}, m^2_{23} and m^2_{13}. The partial width is given by [40]

$$\Gamma(0\to 1,2,3)=\frac{1}{(2\pi)^3}\frac{1}{32M_0^3}\int^{\left(m^2_{12}\right)_{\max}}_{\left(m^2_{12}\right)_{\min}}dm^2_{12}\int^{\left(m^2_{23}\right)_{\max}}_{\left(m^2_{23}\right)_{\min}}dm^2_{23}|\overline{\mathbf{M}}|^2\,, \tag{B.8}$$

where

- $(m^2_{12})_{\max}=(M_0-m_3)^2$,

- $(m_{12}^2)_{\rm min} = (m_1 + m_2)^2$,
- $(m_{23}^2)_{\rm max} = (E_2^* + E_3^*)^2 - \left(\sqrt{E_2^{*2} - m_2^2} - \sqrt{E_3^{*2} - m_3^2}\right)$
- $(m_{23}^2)_{\rm min} = (E_2^* + E_3^*)^2 - \left(\sqrt{E_2^{*2} - m_2^2} + \sqrt{E_3^{*2} - m_3^2}\right)$,
- $E_2^* = \left(m_{12}^2 - m_1^2 + m_2^2\right)/2m_{12}$ and $E_3^* = \left(M_0^2 - m_{12}^2 - m_3^2\right)/2m_{12}$ are the energies of particles 2 and 3 in the m_{12} rest frame.

B.3 Charginos

Most of the chargino $\not{R}_{\rm p}$ decay rates have already been calculated in [2] in the case of no left/right mixing for the first two operators in the $\not{R}_{\rm p}$ superpotential. We recalculate these rates with left/right mixing. First we consider the LLE decays of the chargino. There are three possible decay modes:

1. $\tilde{\chi}^+ \to \bar{\nu}_{\rm i}\ell^+_{\rm j}\nu_{\rm k}$,
2. $\tilde{\chi}^+ \to \nu_{\rm i}\nu_{\rm j}\ell^+_{\rm k}$,
3. $\tilde{\chi}^+ \to \ell^+_{\rm i}\ell^+_{\rm j}\ell^-_{\rm k}$.

The Feynman diagrams for these decays are shown in figure 23. The spin averaged matrix elements are given by

$$|\overline{\mathbf{M}}(\tilde{\chi}^+_l \to \bar{\nu}_i\ell^+_j\nu_k)|^2 = \\ = \frac{g^2\lambda^2_{ijk}}{2}\left[\sum_{\alpha=1,2}|L^{2k-1}_{2\alpha}|^2\Psi(\tilde{\ell}^*_{k\alpha},\nu_i,\ell_j,\nu_k) + 2L^{2k-1}_{21}L^{2k-1}_{22}\Upsilon(\tilde{\ell}^*_k,\nu_i,\ell_j,\nu_k)\right], \quad \text{(B.9)}$$

$$|\overline{\mathbf{M}}(\tilde{\chi}^+_l \to \nu_i\nu_j\ell^+_k)|^2 = \\ = \frac{g^2\lambda^2_{ijk}}{2}\left[\sum_{\alpha=1,2}|L^{2i-1}_{1\alpha}|^2\Psi(\tilde{\ell}_{i\alpha},\nu_j,\ell_k,\nu_i) + \sum_{\alpha=1,2}|L^{2j-1}_{1\alpha}|^2\Psi(\tilde{\ell}_{j\alpha},\nu_i,\ell_k,\nu_j)\times\right. \\ \times 2L^{2i-1}_{11}L^{2i-1}_{12}\Upsilon(\tilde{\ell}_i,\nu_j,\ell_k,\nu_i) + 2L^{2j-1}_{11}L^{2j-1}_{12}\Upsilon(\tilde{\ell}_j,\nu_i,\ell_k,\nu_j) + \\ \left. + \sum_{\alpha=1,2}\sum_{\beta=1,2}2L^{2i-1}_{1\alpha}L^{2j-1}_{1\beta}\Phi(\tilde{\ell}_{j\beta},\tilde{\ell}_{i\alpha},\nu_i,\ell_k,\nu_j)\right], \quad \text{(B.10)}$$

$$|\overline{\mathbf{M}}(\tilde{\chi}^+_l \to \ell^+_i\ell^+_j\ell^-_k)|^2 = \frac{g^2\lambda^2_{ijk}}{2}\times \\ \times\left[\Psi(\tilde{\nu}_i,\ell_j,\ell_k,\ell_i) + \Psi(\tilde{\nu}_j,\ell_i,\ell_k,\ell_j) + 2\Phi(\tilde{\nu}_j,\tilde{\nu}_i,\ell_i,\ell_k,\ell_j)\right]. \quad \text{(B.11)}$$

We go beyond the results of [2] to include the decay $\tilde{\chi}^+ \to \bar{\nu}_{\rm i}\ell^+_{\rm j}\nu_{\rm k}$.

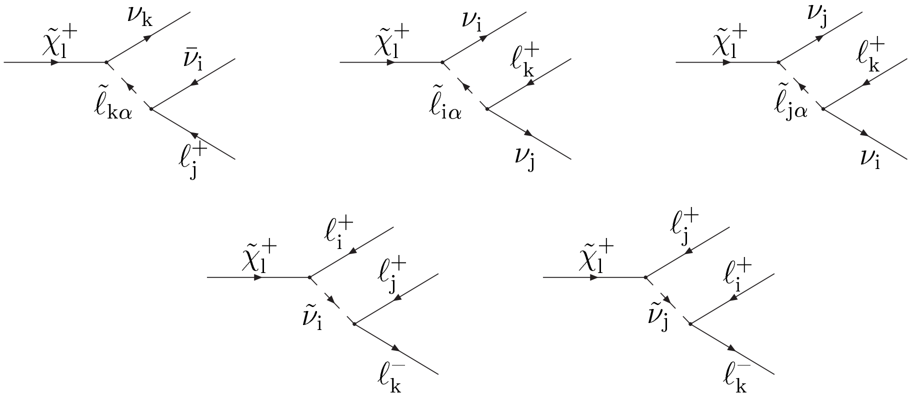

Figure 23: LLE decays of the $\tilde{\chi}^+$.

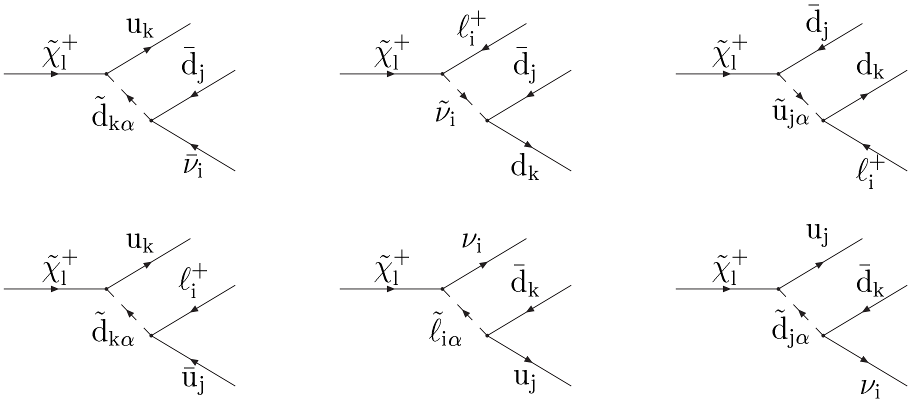

Figure 24: LQD decays of the $\tilde{\chi}^+$.

We now consider the LQD decays of the chargino. There are four possible decay modes:

1. $\tilde{\chi}^+ \to \bar{\nu}_{\rm i}\bar{\rm d}_{\rm j}{\rm u}_{\rm k}$,
2. $\tilde{\chi}^+ \to \ell^+_{\rm i}\bar{\rm u}_{\rm j}{\rm u}_{\rm k}$,
3. $\tilde{\chi}^+ \to \ell^+_{\rm i}\bar{\rm d}_{\rm j}{\rm d}_{\rm k}$,
4. $\tilde{\chi}^+ \to \nu_{\rm i}{\rm u}_{\rm j}\bar{\rm d}_{\rm k}$.

The Feynman diagrams for these decays are shown in figure 24. The spin and colour averaged matrix elements are given below

$$|\overline{\mathbf{M}}(\tilde{\chi}^+_l \to \bar{\nu}_i \bar{d}_j u_k)|^2 = \frac{g^2\lambda'^2_{ijk}N_c}{2} \times$$
$$\times \left[\sum_{\alpha=1,2}|Q^{2k-1}_{2\alpha}|^2\Psi(\tilde{d}^*_{k\alpha},\nu_i,d_j,u_k) + 2Q^{2k-1}_{21}Q^{2k-1}_{22}\Upsilon(\tilde{d}^*_k,\nu_i,d_j,u_k)\right], \quad \text{(B.12)}$$

$$|\overline{\mathbf{M}}(\tilde{\chi}^+_l \to \ell^+_i \bar{u}_j u_k)|^2 = \frac{g^2 \lambda'^2_{ijk} N_c}{2} \times$$
$$\times \left[\sum_{\alpha=1,2} |Q^{2k-1}_{2\alpha}|^2 \Psi(\tilde{d}^*_{k\alpha}, \ell_i, u_j, u_k) + 2Q^{2k-1}_{21} Q^{2k-1}_{22} \Upsilon(\tilde{d}^*_k, \ell_i, u_j, u_k) \right], \quad \text{(B.13)}$$

$$|\overline{\mathbf{M}}(\tilde{\chi}^+_l \to \ell^+_i \bar{d}_j d_k)|^2 = \frac{g^2 \lambda'^2_{ijk} N_c}{2} \times$$
$$\times \Big[\Psi(\tilde{\nu}_i, d_j, d_k, \ell_i) + \sum_{\alpha=1,2} |Q^{2j}_{1\alpha}|^2 \Psi(\tilde{u}_{j\alpha}, \ell_i, d_k, d_j) +$$
$$+ 2Q^{2j}_{11} Q^{2j}_{12} \Upsilon(\tilde{u}_j, \ell_i, d_k, d_j) + 2 \sum_{\alpha=1,2} Q^{2j}_{1\alpha} \Phi(\tilde{u}_{j\alpha}, \tilde{\nu}_i, \ell_i, d_k, d_j) \Big], \quad \text{(B.14)}$$

$$|\overline{\mathbf{M}}(\tilde{\chi}^+_l \to \nu_i u_j \bar{d}_k)|^2 =$$
$$= \frac{g^2 \lambda'^2_{ijk} N_c}{2} \Big[\sum_{\alpha=1,2} |L^{2i-1}_{1\alpha}|^2 \Psi(\tilde{\ell}_{i\alpha}, u_j, d_k, \nu_i) + \sum_{\alpha=1,2} |Q^{2j-1}_{1\alpha}|^2 \Psi(\tilde{d}_{j\alpha}, \nu_i, d_k, u_j) +$$
$$+ 2L^{2i-1}_{11} L^{2i-1}_{12} \Upsilon(\tilde{\ell}_i, u_j, d_k, \nu_i) + 2Q^{2j-1}_{11} Q^{2j-1}_{12} \Upsilon(\tilde{d}_j, \nu_i, d_k, u_j) +$$
$$+ 2 \sum_{\alpha=1,2} \sum_{\beta=1,2} L^{2i-1}_{1\alpha} Q^{2j-1}_{1\beta} \Phi(\tilde{d}_{j\beta}, \tilde{\ell}_{i\alpha}, \nu_i, d_k, u_j) \Big]. \quad \text{(B.15)}$$

We now come to the baryon number violating decays. We do not assume here that there is only one non-zero $\not{R}_p$ coupling. This means that more than one coupling contributes to these decays. It may seem that this will only matter in the case where more than one λ'' coupling is taken to be non zero, however there can be more than one diagram even with only one coupling non zero, e.g. λ''_{112} will give two diagrams for each of the decay modes. In this case one of these diagrams is obtained from the other simply by crossing the identical fermions in the final state.

There are two possible decay modes:

1. $\tilde{\chi}^+ \to u_i u_j d_k$,
2. $\tilde{\chi}^+ \to \bar{d}_i \bar{d}_j \bar{d}_k$.

The Feynman diagrams for these decays are shown in figure 3. The spin and colour averaged matrix elements for these processes with left/right sfermion mixing are given below.

$$|\overline{\mathbf{M}}\ (\tilde{\chi}^+_l \to u_i u_j d_k)|^2 = \frac{g^2 N_c!}{2(1+\delta_{ij})} \times$$
$$\times \Big[\lambda''^2_{jik} \sum_{\alpha=1,2} |Q^{2i-1}_{2\alpha}|^2 \Psi(\tilde{d}^*_{i\alpha}, u_j, d_k, u_i) + \lambda''^2_{ijk} \sum_{\alpha=1,2} |Q^{2j-1}_{2\alpha}|^2 \Psi(\tilde{d}^*_{j\alpha}, u_i, d_k, u_j) +$$

Coefficient		Coefficient	
$a(\tilde{\ell}_{i\alpha})$	0	$b(\tilde{\ell}_{i\alpha})$	$L^{2i-1}_{1\alpha}U_{l1} - \frac{U_{l2}L^{2i-1}_{2\alpha}m_{e_i}}{\sqrt{2}M_W\cos\beta}$
$a(\tilde{\nu}_i)$	$-\frac{U_{l2}m_{e_i}}{\sqrt{2}M_W\cos\beta}$	$b(\tilde{\nu}_i)$	V^*_{l1}
$a(\tilde{u}_{i\alpha})$	$-\frac{m_{d_i}U_{l2}Q^{2i}_{1\alpha}}{\sqrt{2}M_W\cos\beta}$	$b(\tilde{u}_{i\alpha})$	$V^*_{l1}Q^{2i}_{1\alpha} - \frac{m_{u_i}V^*_{l2}Q^{2i}_{2\alpha}}{\sqrt{2}M_W\sin\beta}$
$a(\tilde{d}_{i\alpha})$	$-\frac{m_{u_i}V^*_{l2}Q^{2i-1}_{1\alpha}}{\sqrt{2}M_W\sin\beta}$	$b(\tilde{d}_{i\alpha})$	$Q^{2i-1}_{1\alpha}U_{l1} - \frac{U_{l2}Q^{2i-1}_{2\alpha}m_{d_i}}{\sqrt{2}M_W\cos\beta}$

Table 3: Couplings for the chargino decays.

$$+2\lambda''^2_{jik}Q^{2i-1}_{21}Q^{2i-1}_{22}\Upsilon(\tilde{d}^*_i,u_j,d_k,u_i) + 2\lambda''^2_{ijk}Q^{2j-1}_{21}Q^{2j-1}_{22}\Upsilon(\tilde{d}^*_j,u_i,d_k,u_j) +$$

$$+2\lambda''_{ijk}\lambda''_{jik}\sum_{\alpha=1,2}\sum_{\beta=1,2}Q^{2i-1}_{2\alpha}Q^{2j-1}_{2\beta}\Phi(\tilde{d}^*_{j\beta},\tilde{d}^*_{i\alpha},u_i,d_k,u_j)\Bigg], \tag{B.16}$$

$$|\overline{\mathbf{M}}\ (\tilde{\chi}^+_l \to \bar{d}_i\bar{d}_j\bar{d}_k)|^2 = \frac{g^2N_c!}{2(1+\delta_{ij}+\delta_{jk}+\delta_{ik})}\times$$

$$\times\Bigg[\lambda''^2_{ijk}\sum_{\alpha=1,2}|Q^{2i}_{2\alpha}|^2\Psi(\tilde{u}^*_{i\alpha},d_j,d_k,d_i) + \lambda''^2_{jki}\sum_{\alpha=1,2}|Q^{2j}_{2\alpha}|^2\Psi(\tilde{u}^*_{j\alpha},d_i,d_k,d_j) +$$

$$+\lambda''^2_{kij}\sum_{\alpha=1,2}|Q^{2k}_{2\alpha}|^2\Psi(\tilde{u}^*_{k\alpha},d_i,d_j,d_k) + 2\lambda''^2_{ijk}Q^{2i}_{21}Q^{2i}_{22}\Upsilon(\tilde{u}^*_i,d_j,d_k,d_i) +$$

$$+2\lambda''^2_{jki}Q^{2j}_{21}Q^{2j}_{22}\Upsilon(\tilde{u}^*_j,d_i,d_k,d_j) + 2\lambda''^2_{kij}Q^{2k}_{21}Q^{2k}_{22}\Upsilon(\tilde{u}^*_{k\alpha},d_i,d_j,d_k) -$$

$$-2\lambda''_{ijk}\lambda''_{jki}\sum_{\alpha=1,2}\sum_{\beta=1,2}Q^{2i}_{2\alpha}Q^{2j}_{2\beta}\Phi(\tilde{u}^*_{j\beta},\tilde{u}^*_{i\alpha},d_i,d_k,d_j) -$$

$$-2\lambda''_{ijk}\lambda''_{kij}\sum_{\alpha=1,2}\sum_{\beta=1,2}Q^{2i}_{2\alpha}Q^{2k}_{2\beta}\Phi(\tilde{u}^*_{k\beta},\tilde{u}^*_{i\alpha},d_i,d_j,d_k) -$$

$$-2\lambda''_{jki}\lambda''_{kij}\sum_{\alpha=1,2}\sum_{\beta=1,2}Q^{2j}_{2\alpha}Q^{2k}_{2\beta}\Phi(\tilde{u}^*_{k\beta},\tilde{u}^*_{j\alpha},d_j,d_i,d_k)\Bigg]. \tag{B.17}$$

The coefficients in the chargino matrix elements are given in table 3 and the partial widths can be obtained by integrating the matrix elements in the same way as for the neutralino decays.

Again when the chargino mass matrix is diagonalized negative eigenvalues can be obtained and the fields must be rotated. This means here that the coefficients $b(\tilde{\nu}_i)$, $b(\tilde{u}_{i\alpha})$ and $b(\tilde{d}_{i\alpha})$ change sign if the chargino mass is negative.

B.4 Gluinos

These decay rates are calculated here with left/right mixing. There are three possible decay modes, two via the LQD operator and one via the UDD operator:

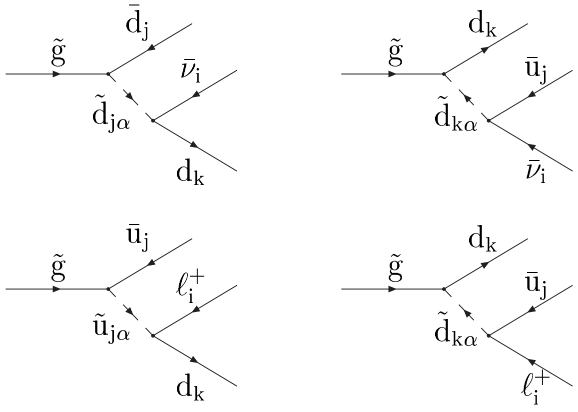

Figure 25: LQD decays of the $\tilde{\mathrm{g}}$.

1. $\tilde{\mathrm{g}} \to \bar{\nu}_{\mathrm{i}} \bar{\mathrm{d}}_{\mathrm{j}} \mathrm{d}_{\mathrm{k}}$,
2. $\tilde{\mathrm{g}} \to \ell^+_{\mathrm{i}} \bar{\mathrm{u}}_{\mathrm{j}} \mathrm{d}_{\mathrm{k}}$,
3. $\tilde{\mathrm{g}} \to \mathrm{u}_{\mathrm{i}} \mathrm{u}_{\mathrm{j}} \mathrm{d}_{\mathrm{k}}$.

Since the gluino is a Majorana fermion the charge conjugate decay modes are possible as well. The Feynman diagrams for these processes are in figures 25 and 5, respectively. The spin and colour averaged matrix elements with left/right sfermion mixing are given below

$$
\begin{aligned}
&|\overline{\mathbf{M}}(\tilde{g} \to \bar{\nu}_i \bar{d}_j d_k)|^2 = \\
&= \frac{\lambda'^2_{ijk} g_s^2}{2} \Bigg[\sum_{\alpha=1,2} |Q^{2j-1}_{1\alpha}|^2 \Psi(\tilde{d}_{j\alpha}, \nu_i, d_k, d_j) + \sum_{\alpha=1,2} |Q^{2k-1}_{2\alpha}|^2 \Psi(\tilde{d}^*_{k\alpha}, \nu_i, d_j, d_k) + \\
&\qquad + 2Q^{2j-1}_{11} Q^{2j-1}_{12} \Upsilon(\tilde{d}_j, \nu_i, d_k, d_j) + 2Q^{2k-1}_{21} Q^{2k-1}_{22} \Upsilon(\tilde{d}^*_k, \nu_i, d_j, d_k) - \\
&\qquad - \sum_{\alpha=1,2} \sum_{\beta=1,2} 2Q^{2j-1}_{1\alpha} Q^{2k-1}_{2\beta} \Phi(\tilde{d}^*_{k\beta}, \tilde{d}_{j\alpha}, d_j, \nu_i, d_k) \Bigg],
\end{aligned} \tag{B.18}
$$

$$
\begin{aligned}
&|\overline{\mathbf{M}}(\tilde{g} \to \ell^+_i \bar{u}_j d_k)|^2 = \\
&= \frac{\lambda'^2_{ijk} g_s^2}{2} \Bigg[\sum_{\alpha=1,2} |Q^{2j}_{1\alpha}|^2 \Psi(\tilde{u}_{j\alpha}, \ell_i, d_k, u_j) + 2Q^{2j}_{11} Q^{2j}_{12} \Upsilon(\tilde{u}_j, \ell_i, d_k, u_j) + \\
&\qquad + \sum_{\alpha=1,2} |Q^{2k-1}_{2\alpha}|^2 \Psi(\tilde{d}^*_{k\alpha}, \ell_i, u_j, d_k) + 2Q^{2k-1}_{21} Q^{2k-1}_{22} \Upsilon(\tilde{d}^*_k, \ell_i, u_j, d_k) - \\
&\qquad - \sum_{\alpha=1,2} \sum_{\beta=1,2} 2Q^{2j}_{1\alpha} Q^{2k-1}_{2\beta} \Phi(\tilde{d}^*_{k\beta}, \tilde{u}_{j\alpha}, u_j, \ell_i, d_k) \Bigg],
\end{aligned} \tag{B.19}
$$

Coefficient		Coefficient	
$a(\tilde{u}_{i\alpha})$	$Q^{2i}_{2\alpha}$	$b(\tilde{u}_{i\alpha})$	$-Q^{2i}_{1\alpha}$
$a(\tilde{d}_{i\alpha})$	$Q^{2i-1}_{2\alpha}$	$b(\tilde{d}_{i\alpha})$	$-Q^{2i-1}_{1\alpha}$

Table 4: Couplings for the gluino decays.

$$
\begin{aligned}
&|\overline{\mathbf{M}}(\tilde{g} \to \bar{u}_i \bar{d}_j \bar{d}_k)|^2 = \\
&= \frac{{\lambda''}^2_{ijk}(N_c-1)!}{2} \Bigg[\sum_{\alpha=1,2} |Q^{2i}_{2\alpha}|^2 \Psi(\tilde{u}^*_{i\alpha}, d_j, d_k, u_i) + 2Q^{2i}_{21}Q^{2i}_{22}\Upsilon(\tilde{u}^*_i, d_j, d_k, u_i) + \\
&\quad + \sum_{\alpha=1,2} |Q^{2j-1}_{2\alpha}|^2 \Psi(\tilde{d}^*_{j\alpha}, u_i, d_k, d_j) + 2Q^{2j-1}_{21}Q^{2j-1}_{22}\Upsilon(\tilde{d}^*_j, u_i, d_k, d_j) + \\
&\quad + \sum_{\alpha=1,2} |Q^{2k-1}_{2\alpha}|^2 \Psi(\tilde{d}^*_{k\alpha}, u_i, d_j, d_k) + 2Q^{2k-1}_{21}Q^{2k-1}_{22}\Upsilon(\tilde{d}^*_k, u_i, d_j, d_k) + \\
&\quad + \frac{1}{N_c-1} \sum_{\alpha=1,2}\sum_{\beta=1,2} Q^{2i}_{2\alpha}Q^{2j-1}_{2\beta}\Phi(\tilde{d}^*_{j\beta}, \tilde{u}^*_{i\alpha}, u_i, d_k, d_j) + \\
&\quad + \frac{1}{N_c-1} \sum_{\alpha=1,2}\sum_{\beta=1,2} Q^{2i}_{2\alpha}Q^{2k-1}_{2\beta}\Phi(\tilde{d}^*_{k\beta}, \tilde{u}^*_{i\alpha}, u_i, d_j, d_k) + \\
&\quad + \frac{1}{N_c-1} \sum_{\alpha=1,2}\sum_{\beta=1,2} Q^{2j-1}_{2\alpha}Q^{2k-1}_{2\beta}\Phi(\tilde{d}^*_{k\beta}, \tilde{d}^*_{j\alpha}, d_j, u_i, d_k) \Bigg] . \qquad \text{(B.20)}
\end{aligned}
$$

The coefficients for these matrix elements are given in table 4. As the gluino mass is not obtained by diagonalising a mass matrix it cannot be negative.

C. Hard processes

All of the single neutralino, chargino and gluino production cross sections can be obtained by crossing from the decay matrix elements we have already presented in appendix B. This crossing will lead to the invariants m^2_{12}, m^2_{23} and m^2_{13} being replaced by the usual invariants s, t and u. There is an overall sign change due to exchanging fermions between the initial and final states. It should also be remembered that the decay matrix elements given have been averaged over the spin and colour of the initial particle. The cross-sections for the remaining processes are presented below. In all cases the formulae have been averaged over the initial spins and colours. The initial state masses have all been set to zero, except where they appear in a coupling constant. In t- and u-channel fermion propagators the fermion masses have been neglected as well.

Slepton couplings			
$Z_{\nu_i}^{\alpha\beta}$	$-\frac{1}{2}\delta_{\alpha=1,\beta=1}$	$Z_{\ell_i}^{\alpha\beta}$	$\frac{1}{2}\left(L_{1\alpha}^{2i-1}L_{1\beta}^{2i-1}-2\sin^2\theta_w\delta_{\alpha\beta}\right)$
Squark couplings			
$Z_{u_i}^{\alpha\beta}$	$\frac{1}{2}\left(-Q_{1\alpha}^{2i}Q_{1\beta}^{2i}+2e_u\sin^2\theta_w\delta_{\alpha\beta}\right)$	$Z_{d_i}^{\alpha\beta}$	$\frac{1}{2}\left(Q_{1\alpha}^{2i-1}Q_{1\beta}^{2i-1}+2e_d\sin^2\theta_w\delta_{\alpha\beta}\right)$
Quark couplings			
Z_{u_L} Z_{u_R}	$-\frac{1}{4}\left(1-2e_u\sin^2\theta_w\right)$ $\frac{1}{2}e_u\sin^2\theta_w$	Z_{d_L} Z_{d_R}	$\frac{1}{4}\left(1+2e_d\sin^2\theta_w\right)$ $\frac{1}{2}e_d\sin^2\theta_w$

Table 5: Couplings of sleptons, squarks and quarks to the Z^0.

C.1 LQD processes

C.1.1 Resonant slepton followed by weak decay

There are three processes which can occur via the production of a resonant slepton followed by a weak decay of this slepton. These are:

1. $\mathrm{d_j\bar{d}_k} \to \tilde{\ell}^*_{\mathrm{i}}\mathrm{W}^-$,
2. $\mathrm{u_j\bar{d}_k} \to \tilde{\nu}^*_{\mathrm{i}}\mathrm{W}^+$,
3. $\mathrm{u_j\bar{d}_k} \to \tilde{\tau}^*_1\mathrm{Z}^0$.

It should be noted that we have not included processes where the resonance is not accessible, e.g. $\mathrm{u_j\bar{d}_k} \to \tilde{\tau}^*_2\mathrm{Z}^0$.

$$
\begin{aligned}
|\overline{\mathbf{M}}(d_j\bar{d}_k \to \tilde{\ell}^*_{i\alpha}W^-)|^2 = {} & \frac{g^2\lambda'^2_{ijk}|L_{1\alpha}^{2i-1}|^2}{2M_W^2N_c}\times \\
& \times\Bigg[\hat{s}^2p_{cm}^2R(\tilde{\nu}_i,\hat{s})+\frac{1}{4\hat{u}^2}\left(2M_W^2(\hat{u}\hat{t}-M^2_{\tilde{\ell}_{i\alpha}}M_W^2)+\hat{u}^2\hat{s}\right)+ \\
& +\frac{\hat{s}\left(\hat{s}-M^2_{\tilde{\nu}_i}\right)R(\tilde{\nu}_i,\hat{s})}{2\hat{u}}\left(M_W^2(2M^2_{\tilde{\ell}_{i\alpha}}-\hat{u})+\hat{u}(\hat{s}-M^2_{\tilde{\ell}_{i\alpha}})\right)\Bigg],
\end{aligned} \tag{C.1}
$$

$$
\begin{aligned}
|\overline{\mathbf{M}}(u_j\bar{d}_k \to \tilde{\nu}^*_iW^+)|^2 = {} & \frac{g^2\lambda'^2_{ijk}}{2M_W^2N_c}\times \\
& \times\Bigg[\sum_{\alpha=1,2}|L_{1\alpha}^{2i-1}|^4\hat{s}^2p_{cm}^2R(\tilde{\ell}_{i\alpha},\hat{s})+2|L_{11}^{2i-1}|^2|L_{12}^{2i-1}|^2\hat{s}^2p_{cm}^2S(\tilde{\ell}_{i1},\tilde{\ell}_{i2},\hat{s},\hat{s})+ \\
& +\frac{1}{4\hat{u}^2}\left(2M_W^2(\hat{u}\hat{t}-M^2_{\tilde{\nu}_i}M_W^2)+\hat{u}^2\hat{s}\right)+ \\
& +\frac{|L_{1\alpha}^{2i-1}|^2\hat{s}\left(\hat{s}-M^2_{\tilde{\ell}_{i\alpha}}\right)R(\tilde{\ell}_{i\alpha},\hat{s})}{2\hat{u}}\left(M_W^2(2M^2_{\tilde{\nu}_i}-\hat{u})+\hat{u}(\hat{s}-M^2_{\tilde{\nu}_i})\right)\Bigg],
\end{aligned} \tag{C.2}
$$

$$
\begin{aligned}
|\overline{\mathbf{M}}(u_j\bar{d}_k \to \tilde{\ell}^*_{i1}Z^0)|^2 = & \frac{g^2\lambda'^2_{ijk}}{N_cM_Z^2\cos^2\theta_w}\times \\
\times \Bigg[& \sum_{\alpha=1,2}|L^{2i-1}_{1\alpha}|^2|Z^{\alpha1}_{\ell_i}|^2\hat{s}^2p^2_{cm}R(\tilde{\ell}_{i\alpha},\hat{s}^2)+ \\
& + 2L^{2i-1}_{11}L^{2i-1}_{12}Z^{11}_{\ell_i}Z^{21}_{\ell_i}\hat{s}^2p^2_{cm}S(\tilde{\ell}_{i1},\tilde{\ell}_{i2},\hat{s},\hat{s}) + \\
& + \frac{|L^{2i-1}_{11}|^2Z^2_{u_L}}{\hat{u}^2}\left(2M_Z^2(\hat{u}\hat{t}-M^2_{\tilde{\ell}_{i1}}M_Z^2)+\hat{u}^2\hat{s}\right) + \\
& + \frac{|L^{2i-1}_{11}|^2Z^2_{d_R}}{\hat{t}^2}\left(2M_Z^2(\hat{u}\hat{t}-M^2_{\tilde{\ell}_{i1}}M_Z^2)+\hat{t}^2\hat{s}\right) + \\
& + \sum_{\alpha=1,2}\frac{L^{2i-1}_{1\alpha}L^{2i-1}_{11}Z^{\alpha1}_{\ell_i}Z_{u_L}\hat{s}\left(\hat{s}-M^2_{\tilde{\ell}_{i\alpha}}\right)R(\tilde{\ell}_{i\alpha},\hat{s}^2)}{\hat{u}}\times \\
& \qquad \times\left(M_Z^2(2M^2_{\tilde{\ell}_{i1}}-\hat{u})+\hat{u}(s-M^2_{\tilde{\ell}_{i1}})\right) + \\
& + \sum_{\alpha=1,2}\frac{L^{2i-1}_{1\alpha}L^{2i-1}_{11}Z^{\alpha1}_{\ell_i}Z_{d_R}\hat{s}\left(\hat{s}-M^2_{\tilde{\ell}_{i\alpha}}\right)R(\tilde{\ell}_{i\alpha},\hat{s}^2)}{\hat{t}}\times \\
& \qquad \times\left(M_Z^2(2M^2_{\tilde{\ell}_{i1}}-\hat{t})+\hat{t}(s-M^2_{\tilde{\ell}_{i1}})\right) - \\
& - \frac{2|L^{2i-1}_{11}|^2Z_{u_L}Z_{d_R}}{\hat{u}\hat{t}}\left(2M_Z^2(M^2_{\tilde{\ell}_{i1}}-\hat{t})(M^2_{\tilde{\ell}_{i1}}-\hat{u})-\hat{s}\hat{t}\hat{u}\right)\Bigg], \qquad \text{(C.3)}
\end{aligned}
$$

where in all the above equations

$$
p^2_{cm} = \frac{1}{4\hat{s}^2}\left[\hat{s}-(m_1+m_2)^2\right]\left[\hat{s}-(m_1-m_2)^2\right], \qquad \text{(C.4)}
$$

and m_1, m_2 are the masses of the final state particles.

C.1.2 Resonant slepton followed by $\not{R}_p$ decay

There are four process it which we can produce a resonant slepton via $\not{R}_p$ which then decays back to Standard Model particles via a $\not{R}_p$ decay. These are:

1. $\mathrm{d_j\bar{d}_k \to d_l\bar{d}_m}$,
2. $\mathrm{u_j\bar{d}_k \to u_l\bar{d}_m}$,
3. $\mathrm{d_j\bar{d}_k} \to \ell^-_\mathrm{l}\ell^+_\mathrm{m}$,
4. $\mathrm{u_j\bar{d}_k} \to \nu_\mathrm{l}\ell^+_\mathrm{m}$.

The first two of these process only require non-zero LQD couplings whereas the second two require both non-zero LQD and LLE couplings. The matrix elements are presented below for an arbitrary number of non-zero $\not{R}_p$ couplings

$$
\begin{aligned}
|\overline{\mathbf{M}}(d_j\bar{d}_k \to d_l\bar{d}_m)|^2 =& \frac{1}{4}\sum_{i,n=1,3} \lambda'_{ijk}\lambda'_{ilm}\lambda'_{njk}\lambda'_{nlm} S(\tilde{\nu}_i,\tilde{\nu}_n,\hat{s},\hat{s})\hat{s}\left(\hat{s}-m^2_{d_l}-m^2_{d_m}\right)+ \\
&+\frac{1}{4}\sum_{i,n=1,3} \lambda'_{ijl}\lambda'_{ikm}\lambda'_{njl}\lambda'_{nkm}\frac{(m^2_{d_l}-\hat{t})(m^2_{d_m}-\hat{t})}{(\hat{t}-M^2_{\tilde{\nu}_i})(\hat{t}-M^2_{\tilde{\nu}_n})}\,, \qquad \text{(C.5)}
\end{aligned}
$$

$$
\begin{aligned}
|\overline{\mathbf{M}}(u_j\bar{d}_k \to u_l\bar{d}_m)|^2 =& \frac{1}{4}\sum_{\alpha,\beta=1,2}\sum_{i,n=1,3} \lambda'_{ijk}\lambda'_{ilm}\lambda'_{njk}\lambda'_{nlm}|L^{2i-1}_{1\alpha}|^2|L^{2n-1}_{1\beta}|^2\times \\
&\times S(\tilde{\ell}_{i\alpha},\tilde{\ell}_{n\beta},\hat{s},\hat{s})\hat{s}\left(\hat{s}-m^2_{u_l}-m^2_{d_m}\right)\,, \qquad \text{(C.6)}
\end{aligned}
$$

$$
|\overline{\mathbf{M}}(d_j\bar{d}_k \to \ell^-_l\ell^+_m)|^2 = \frac{1}{4N_c}\sum_{i,n=1,3} \lambda'_{ijk}\lambda'_{njk}\lambda_{ilm}\lambda_{nlm} S(\tilde{\nu}_i,\tilde{\nu}_n,\hat{s},\hat{s})\hat{s}\left(\hat{s}-m^2_{\ell_m}-m^2_{\ell_l}\right) \qquad \text{(C.7)}
$$

$$
\begin{aligned}
|\overline{\mathbf{M}}(u_j\bar{d}_k \to \nu_l\ell^+_m)|^2 =& \frac{1}{4N_c}\sum_{\alpha,\beta=1,2}\sum_{i,n=1,3} \lambda'_{ijk}\lambda'_{njk}\lambda_{ilm}\lambda_{nlm}|L^{2i-1}_{1\alpha}|^2|L^{2n-1}_{1\beta}|^2\times \\
&\times S(\tilde{\ell}_{i\alpha},\tilde{\ell}_{n\beta},\hat{s},\hat{s})\hat{s}\left(\hat{s}-m^2_{\ell_m}\right)\,. \qquad \text{(C.8)}
\end{aligned}
$$

C.1.3 Resonant slepton production followed by Higgs decay

There are a number of processes which can occur via the production of a resonant slepton which can then decay to either a neutral or charged Higgs:

1. $\mathrm{u_j\bar{d}_k} \to \tilde{\ell}^*_{\mathrm{i}\beta}\mathrm{h_0/H_0/A_0}$,
2. $\mathrm{d_j\bar{d}_k} \to \tilde{\ell}^*_{\mathrm{i}\alpha}\mathrm{H^-}$,
3. $\mathrm{u_j\bar{d}_k} \to \tilde{\nu}^*_{\mathrm{i}}\mathrm{H^+}$.

As we only include processes where there is a possibility of a resonant production mechanism, the process $\mathrm{d_j\bar{d}_k} \to \tilde{\nu}^*_{\mathrm{i}}\mathrm{h_0/H_0/A_0}$ is not included. For the same reason we also have not included the processes $\mathrm{u_j\bar{d}_k} \to \tilde{\ell}^*_{\mathrm{iL}}\mathrm{h_0/H_0/A_0}$ for the first two slepton generations. This is because HERWIG does not include mixing for the first two generation sleptons and the initial state only couples to the left-handed slepton. The process $\mathrm{u_j\bar{d}_k} \to \tilde{\ell}^*_{\mathrm{i2}}\mathrm{h_0/H_0/A_0}$ is also not included for the third generation ($i = 3$) as there is no accessible resonance.

The matrix elements for these processes are given below. Since the matrix elements have the same form for all the neutral Higgs processes we use the notation $\mathrm{H^l_0}$ where $l = 1, 2, 3$ is $\mathrm{h_0}$, $\mathrm{H_0}$ and $\mathrm{A_0}$.

U_i^1	$\frac{m_{u_i}\cos\alpha}{2M_W\sin\beta}$	D_i^1	$-\frac{m_{d_i}\sin\alpha}{2M_W\cos\beta}$
U_i^2	$\frac{m_{u_i}\sin\alpha}{2M_W\sin\beta}$	D_i^2	$\frac{m_{d_i}\cos\alpha}{2M_W\cos\beta}$
U_i^3	$\frac{m_{u_i}\cot\beta}{2M_W}$	D_i^3	$\frac{m_{d_i}\tan\beta}{2M_W}$
U_i^c	$\frac{m_{u_i}\cot\beta}{2\sqrt{2}M_W}$	D_i^c	$\frac{m_{d_i}\tan\beta}{2\sqrt{2}M_W}$

Table 6: Higgs couplings to quarks.

Coefficient	
$H^1_{\tilde{\ell}_{i\alpha}\tilde{\ell}_{i\beta}}$	$-\frac{M_Z\sin(\alpha+\beta)}{\cos\theta_w}\left[L^{2i-1}_{1\alpha}L^{2i-1}_{1\beta}(\frac{1}{2}-\sin^2\theta_w)+\sin^2\theta_w L^{2i-1}_{2\alpha}L^{2i-1}_{2\beta}\right]$ $+\frac{m^2_{e_i}\sin\alpha}{M_W\cos\beta}\left[L^{2i-1}_{1\alpha}L^{2i-1}_{1\beta}+L^{2i-1}_{2\alpha}L^{2i-1}_{2\beta}\right]$ $+\frac{m_{e_i}}{2M_W\cos\beta}(\mu\cos\alpha+A_{e_i}\sin\alpha)\left[L^{2i-1}_{2\alpha}L^{2i-1}_{1\beta}+L^{2i-1}_{1\alpha}L^{2i-1}_{2\beta}\right]$
$H^2_{\tilde{\ell}_{i\alpha}\tilde{\ell}_{i\beta}}$	$\frac{M_Z\cos(\alpha+\beta)}{\cos\theta_w}\left[L^{2i-1}_{1\alpha}L^{2i-1}_{1\beta}(\frac{1}{2}-\sin^2\theta_w)+\sin^2\theta_w L^{2i-1}_{2\alpha}L^{2i-1}_{2\beta}\right]$ $-\frac{m^2_{e_i}\cos\alpha}{M_W\cos\beta}\left[L^{2i-1}_{1\alpha}L^{2i-1}_{1\beta}+L^{2i-1}_{2\alpha}L^{2i-1}_{2\beta}\right]$ $+\frac{m_{e_i}}{2M_W\cos\beta}(\mu\sin\alpha-A_{e_i}\cos\alpha)\left[L^{2i-1}_{2\alpha}L^{2i-1}_{1\beta}+L^{2i-1}_{1\alpha}L^{2i-1}_{2\beta}\right]$
$H^3_{\tilde{\ell}_{i\alpha}\tilde{\ell}_{i\beta}}$	$-\delta_{\alpha\neq\beta}\frac{m_{e_i}}{2M_W}(\mu+A_{e_i}\tan\beta)$
$H^c_{\tilde{\nu}\tilde{\ell}_{i\alpha}}$	$\frac{1}{\sqrt{2}M_W}\left[L^{2i-1}_{1\alpha}\left(m^2_{e_i}\tan\beta-M^2_W\sin 2\beta\right)+L^{2i-1}_{2\alpha}m_{e_i}(\mu+\tan\beta A_{e_i})\right]$

Table 7: Higgs couplings to sleptons.

$$|\overline{\mathbf{M}}(d_j\bar{d}_k\to\tilde{\ell}^*_{i\alpha}H^-)|^2 = \\ =\frac{g^2\lambda'^2_{ijk}}{4N_c}\left[|H^c_{\tilde{\nu}\tilde{\ell}_{i\alpha}}|^2\hat{s}R(\tilde{\nu}_i,\hat{s})+\frac{4|L^{2i-1}_{1\alpha}|^2|D^c_j|^2}{\hat{u}^2}\left(\hat{u}\hat{t}-M^2_{\tilde{\ell}_{i\beta}}M^2_{H^-}\right)\right], \tag{C.9}$$

$$|\overline{\mathbf{M}}(u_j\bar{d}_k\to\tilde{\nu}^*_iH^+)|^2 = \\ =\frac{g^2\lambda'^2_{ijk}\hat{s}}{4N_c}\left[\sum_{\alpha=1,2}|L^{2i-1}_{i\alpha}|^2|H^c_{\tilde{\nu}\tilde{\ell}_{i\alpha}}|^2\hat{s}R(\tilde{\ell}_{i\alpha})+2L^{2i-1}_{i1}L^{2i-1}_{i2}H^c_{\nu\tilde{\ell}_{i1}}H^c_{\nu\tilde{\ell}_{i2}}\hat{s}S(\tilde{\ell}_{i1},\tilde{\ell}_{i2},\hat{s},\hat{s})+\right. \\ \left.+\frac{4|U^c_j|^2}{\hat{u}^2}\left(\hat{u}\hat{t}-M^2_{\tilde{\nu}_i}M^2_{H^+}\right)\right], \tag{C.10}$$

$$|\overline{\mathbf{M}}(u_j\bar{d}_k\to\tilde{\ell}^*_{i\beta}H^l_0)|^2 = \\ =\frac{g^2\lambda'^2_{ijk}}{4N_c}\left[\sum_{\alpha=1,2}|L^{2i-1}_{i\alpha}|^2|H^l_{\tilde{\ell}_{i\alpha}\tilde{\ell}_{i\beta}}|^2\hat{s}R(\tilde{\ell}_{i\alpha})+\right. \\ +2L^{2i-1}_{i1}L^{2i-1}_{i2}H^l_{\tilde{\ell}_{i1}\tilde{\ell}_{i\beta}}H^l_{\tilde{\ell}_{i2}\tilde{\ell}_{i\beta}}\hat{s}S(\tilde{\ell}_{i1},\tilde{\ell}_{i2},\hat{s},\hat{s})+ \tag{C.11} \\ \left.+\frac{|L^{2i-1}_{1\beta}|^2|D^l_j|^2}{\hat{u}^2}\left(\hat{u}\hat{t}-M^2_{\tilde{\ell}_{i\beta}}M^2_{H^l_0}\right)+\frac{|L^{2i-1}_{1\beta}|^2|D^l_k|^2}{\hat{t}^2}\left(\hat{u}\hat{t}-M^2_{\tilde{\ell}_{i\beta}}M^2_{H^l_0}\right)\right].$$

The couplings involved in the various processes can be found in tables 6 and 7.

C.2 UDD processes

C.2.1 Resonant squark followed by weak decay

There are four process which can occur via the production of a resonant squark followed by a weak decay of this squark:

1. $\mathrm{d_j d_k} \to \tilde{\mathrm{d}}_\mathrm{i}^* \mathrm{W}^-$,
2. $\mathrm{d_j d_k} \to \tilde{\mathrm{t}}_1^* \mathrm{Z}^0$,
3. $\mathrm{u_i d_j} \to \tilde{\mathrm{u}}_\mathrm{k}^* \mathrm{W}^+$,
4. $\mathrm{u_i d_j} \to \tilde{\mathrm{b}}_1^* \mathrm{Z}^0$.

Again we do not include processes where the resonance is not accessible, i.e. $\mathrm{d_j d_k} \to \tilde{\mathrm{t}}_2^* \mathrm{Z}^0$ and $\mathrm{u_i d_j} \to \tilde{\mathrm{b}}_2^* \mathrm{Z}^0$. So the matrix elements for these processes are given by

$$
\begin{aligned}
|\overline{\mathbf{M}}(d_j d_k \to \tilde{d}^*_{i\beta} W^-)|^2 &= \frac{g^2 \lambda''^2_{ijk}(N_c-1)!|Q^{2i-1}_{1\beta}|^2 \hat{s}^2 p^2_{cm}}{2N_c M_W^2} \times \\
&\times \left[\sum_{\alpha=1,2} |Q^{2i}_{2\alpha}|^2 |Q^{2i}_{1\alpha}|^2 R(\tilde{u}_{i\alpha},\hat{s}) + 2Q^{2i}_{21}Q^{2i}_{22}Q^{2i}_{11}Q^{2i}_{12} S(\tilde{u}_{i1},\tilde{u}_{i2},\hat{s},\hat{s})\right], \qquad \text{(C.12)}
\end{aligned}
$$

$$
\begin{aligned}
|\overline{\mathbf{M}}(u_i d_j \to \tilde{u}^*_{k\beta} W^+)|^2 &= \frac{g^2 \lambda''^2_{ijk}(N_c-1)!\hat{s}^2 p^2_{cm}|Q^{2i}_{1\beta}|^2}{2N_c M_W^2} \times \\
&\times \left[|Q^{2i-1}_{2\alpha}|^2 |Q^{2i-1}_{1\alpha}|^2 R(\tilde{d}_{k\alpha},\hat{s}) + 2Q^{2i-1}_{21}Q^{2i-1}_{22}Q^{2i-1}_{11}Q^{2i-1}_{12} S(\tilde{d}_{k1},\tilde{d}_{k2},\hat{s},\hat{s})\right], \qquad \text{(C.13)}
\end{aligned}
$$

$$
\begin{aligned}
|\overline{\mathbf{M}}(d_j d_k \to \tilde{u}^*_{i1} Z^0)|^2 &= \frac{g^2 \lambda''^2_{ijk}(N_c-1)!}{N_c M_Z^2 \cos^2\theta_w} \times \\
\times \Bigg[& \sum_{\alpha=1,2} |Q^{2i}_{2\alpha}|^2 |Z^{\alpha 1}_{u_i}|^2 \hat{s}^2 p^2_{cm} R(\tilde{u}_{i\alpha},\hat{s}^2) + 2Q^{2i}_{21}Q^{2i}_{22} Z^{11}_{u_i} Z^{21}_{u_i} \hat{s}^2 p^2_{cm} S(\tilde{u}_{i1},\tilde{u}_{i2},\hat{s},\hat{s}) + \\
& + \frac{|Q^{2i}_{21}|^2 Z^2_{d_R}}{\hat{u}^2}\left(2M_Z^2(\hat{u}\hat{t} - M^2_{\tilde{u}_{i1}} M_Z^2) + \hat{u}^2 \hat{s}\right) + \\
& + \frac{|Q^{2i}_{21}|^2 Z^2_{d_R}}{\hat{t}^2}\left(2M_Z^2(\hat{u}\hat{t} - M^2_{\tilde{u}_{i1}} M_Z^2) + \hat{t}^2 \hat{s}\right) + \\
& + \sum_{\alpha=1,2} \frac{Q^{2i}_{2\alpha}Q^{2i}_{21} Z^{\alpha 1}_{u_i} Z_{d_R}}{\hat{u}} \hat{s}(\hat{s} - M^2_{\tilde{u}_{i\alpha}}) R(\tilde{u}_{i\alpha},\hat{s}^2) \times \\
& \qquad \times \left(M_Z^2(2M^2_{\tilde{u}_{i1}} - \hat{u}) + \hat{u}(\hat{s} - M^2_{\tilde{u}_{i1}})\right) + \\
& + \sum_{\alpha=1,2} \frac{Q^{2i}_{2\alpha}Q^{2i}_{21} Z^{\alpha 1}_{u_i} Z_{d_R}}{\hat{t}} \hat{s}(\hat{s} - M^2_{\tilde{u}_{i\alpha}}) R(\tilde{u}_{i\alpha},\hat{s}^2) \times \\
& \qquad \times \left(M_Z^2(2M^2_{\tilde{u}_{i1}} - \hat{t}) + \hat{t}(\hat{s} - M^2_{\tilde{u}_{i1}})\right) - \\
& - \frac{2|Q^{2i}_{21}|^2}{\hat{u}\hat{t}}\left(2M_Z^2(M^2_{\tilde{u}_{i1}} - \hat{u})(M^2_{\tilde{u}_{i1}} - \hat{t}) - \hat{s}\hat{t}\hat{u}\right)\Bigg], \qquad \text{(C.14)}
\end{aligned}
$$

$$
\begin{aligned}
|\overline{\mathbf{M}}(u_i d_k \to \tilde{d}^*_{j1} Z^0)|^2 = {} & \frac{g^2 {\lambda''}^2_{ijk}(N_c-1)!}{N_c M_Z^2 \cos^2\theta_w} \times \\
& \times \Bigg[\sum_{\alpha=1,2} |Q^{2j-1}_{2\alpha}|^2 |Z^{\alpha 1}_{d_j}|^2 \hat{s}^2 p^2_{cm} R(\tilde{d}_{j\alpha}, \hat{s}^2) + \\
& \quad + 2 Q^{2j-1}_{21} Q^{2j-1}_{22} Z^{11}_{d_j} Z^{21}_{d_j} \hat{s}^2 p^2_{cm} S(\tilde{d}_{j1}, \tilde{d}_{j2}, \hat{s}^2, \hat{s}^2) + \\
& \quad + \frac{|Q^{2i-1}_{21}|^2 Z^2_{u_R}}{\hat{u}^2} \left(2M_Z^2(\hat{u}\hat{t} - M^2_{\tilde{d}_{j1}} M_Z^2) + \hat{u}^2 \hat{s} \right) + \\
& \quad + \frac{|Q^{2i-1}_{21}|^2 Z^2_{d_R}}{\hat{t}^2} \left(2M_Z^2(\hat{u}\hat{t} - M^2_{\tilde{d}_{j1}} M_Z^2) + \hat{t}^2 \hat{s} \right) + \\
& \quad + \sum_{\alpha=1,2} \frac{Q^{2i-1}_{2\alpha} Q^{2i-1}_{21} Z^{\alpha 1}_{d_j} Z_{u_R}}{\hat{u}} \hat{s}(\hat{s} - M^2_{\tilde{d}_{j\alpha}}) R(\tilde{d}_{j\alpha}, \hat{s}^2) \times \\
& \qquad \times \left(M_Z^2 (2M^2_{\tilde{d}_{j1}} - \hat{u}) + \hat{u}(\hat{s} - M^2_{\tilde{d}_{j1}}) \right) + \\
& \quad + \sum_{\alpha=1,2} \frac{Q^{2i-1}_{2\alpha} Q^{2i-1}_{21} Z^{\alpha 1}_{d_j} Z_{d_R}}{\hat{t}} \hat{s}(\hat{s} - M^2_{\tilde{d}_{j\alpha}}) R(\tilde{d}_{j\alpha}, \hat{s}^2) \times \\
& \qquad \times \left(M_Z^2 (2M^2_{\tilde{d}_{j1}} - \hat{t}) + \hat{t}(\hat{s} - M^2_{\tilde{d}_{j1}}) \right) - \\
& \quad - \frac{2|Q^{2i-1}_{21}|^2 Z_{u_R} Z_{d_R}}{\hat{u}\hat{t}} \left(2M_Z^2 (M^2_{\tilde{d}_{j1}} - \hat{u})(M^2_{\tilde{d}_{j1}} - \hat{t}) - \hat{s}\hat{t}\hat{u} \right) \Bigg],
\end{aligned}
\tag{C.15}
$$

where $\hat{s}$ and p_{cm} are as before.

C.2.2 Resonant squark followed by $\not{R}_p$ decay

There are two processes in which a resonant squark is produced via the $\not{B}$ term in the superpotential and these squarks then decay to Standard Model particles:

1. $\mathrm{d_j d_k \to d_l d_m}$,
2. $\mathrm{u_i d_j \to u_l d_m}$.

The matrix elements are given by

$$
\begin{aligned}
& |\overline{\mathbf{M}}(d_j d_k \to d_l d_m)|^2 = \\
& \quad = \frac{(N_c-1)!^2}{4N_c} \sum_{\alpha,\beta=1,2} \sum_{i,n=1,3} {\lambda''}_{ijk} {\lambda''}_{ilm} {\lambda''}_{njk} {\lambda''}_{nlm} |Q^{2i}_{2\alpha}|^2 \times \\
& \qquad \times |Q^{2n}_{2\beta}|^2 S(\tilde{u}_{i\alpha}, \tilde{u}_{n\beta}, \hat{s}, \hat{s}) \hat{s} \left(\hat{s} - m^2_{d_l} - m^2_{d_m} \right),
\end{aligned}
\tag{C.16}
$$

$$
\begin{aligned}
& |\overline{\mathbf{M}}(u_i d_j \to u_l d_m)|^2 = \\
& \quad = \frac{(N_c-1)^2}{4N_c} \sum_{\alpha,\beta=1,2} \sum_{i,n=1,3} {\lambda''}_{ijk} {\lambda''}_{lmk} {\lambda''}_{ijn} {\lambda''}_{lmn} |Q^{2k-1}_{2\alpha}|^2 \times \\
& \qquad \times |Q^{2n-1}_{2\beta}|^2 S(\tilde{d}_{i\alpha}, \tilde{d}_{n\beta}, \hat{s}, \hat{s}) \hat{s} \left(\hat{s} - m^2_{u_l} - m^2_{d_m} \right).
\end{aligned}
\tag{C.17}
$$

C.2.3 Resonant squark production followed by Higgs decay

There are a number of processes which occur via the production of a resonant squark which subsequently decays to either a neutral or charged Higgs. Again we only consider those processes for which a resonance is possible, i.e. we neglect the processes $\mathrm{d_jd_k} \to \tilde{\mathrm{u}}^*_{\mathrm{iR}}\mathrm{h_0/H_0/A_0}$ and $\mathrm{u_id_j} \to \tilde{\mathrm{d}}^*_{\mathrm{iR}}\mathrm{h_0/H_0/A_0}$ for the first two generations and the processes $\mathrm{d_jd_k} \to \tilde{\mathrm{t}}^*_{\mathrm{i2}}\mathrm{h_0/H_0/A_0}$ and $\mathrm{u_id_j} \to \tilde{\mathrm{b}}^*_{\mathrm{i2}}\mathrm{h_0/H_0/A_0}$ for the third generation, where we consider left/right mixing as these process cannot occur via a resonant diagram:

1. $\mathrm{d_jd_k} \to \tilde{\mathrm{d}}^*_{\mathrm{i}}\mathrm{H}^-$,
2. $\mathrm{d_jd_k} \to \tilde{\mathrm{u}}^*_{\mathrm{i1}}\mathrm{h_0/H_0/A_0}$,
3. $\mathrm{u_id_j} \to \tilde{\mathrm{u}}^*_{\mathrm{k}}\mathrm{H}^+$,
4. $\mathrm{u_id_j} \to \tilde{\mathrm{d}}^*_{\mathrm{i1}}\mathrm{h_0/H_0/A_0}$.

The matrix elements for these processes are given below. Due to our notation for the squark mixing matrices in the case of no left/right mixing the right squark is denoted as the second mass eigenstate.

$$\begin{aligned}
&|\overline{\mathbf{M}}(d_jd_k \to \tilde{d}^*_{i\beta}H^-)|^2 = \\
&= \frac{g^2(N_c-1)!}{4N_c}\left[\sum_{\alpha=1,2}\lambda''^2_{ijk}|Q^{2i}_{2\alpha}|^2|H^c_{\tilde{u}_{i\alpha}\tilde{d}_{i\beta}}|^2\hat{s}R(\tilde{u}_{i\alpha},\hat{s}) + \right.\\
&\qquad +2\lambda''^2_{ijk}Q^{2i}_{21}Q^{2i}_{22}H^c_{\tilde{u}_{i1}\tilde{d}_{i\beta}}H^c_{\tilde{u}_{i2}\tilde{d}_{i\beta}}\hat{s}S(\tilde{u}_{i1},\tilde{u}_{i2},\hat{s},\hat{s}) + \\
&\qquad +\frac{4\lambda''^2_{jik}|U^c_j|^2|Q^{2i-1}_{2\beta}|^2}{\hat{u}^2}\left(\hat{u}\hat{t}-M^2_{\tilde{d}_{i\beta}}M^2_{H^-}\right) + \\
&\qquad \left. +\frac{4\lambda''^2_{kij}|U^c_k|^2|Q^{2i-1}_{2\beta}|^2}{\hat{t}^2}\left(\hat{u}\hat{t}-M^2_{\tilde{d}_{i\beta}}M^2_{H^-}\right)\right],
\end{aligned} \tag{C.18}$$

$$\begin{aligned}
&|\overline{\mathbf{M}}(u_id_j \to \tilde{u}^*_{k\beta}H^+)|^2 = \\
&= \frac{g^2(N_c-1)!}{4N_c}\left[\sum_{\alpha=1,2}\lambda''^2_{ijk}|Q^{2k-1}_{2\alpha}|^2 H^c_{\tilde{u}_{k\beta}\tilde{d}_{k\alpha}}|^2\hat{s}R(\tilde{d}_{k\alpha},\hat{s}) + \right.\\
&\qquad +2\lambda''^2_{ijk}Q^{2k-1}_{21}Q^{2k-1}_{22}H^c_{\tilde{u}_{k\beta}\tilde{d}_{k1}}H^c_{\tilde{u}_{k\beta}\tilde{d}_{k2}}\hat{s}S(\tilde{d}_{k1},\tilde{d}_{k2},\hat{s},\hat{s}) + \\
&\qquad \left. +\frac{4\lambda''^2_{kij}|D^c_i|^2|Q^{2k-1}_{2\beta}|^2}{\hat{u}^2}\left(\hat{u}\hat{t}-M^2_{\tilde{d}_{k\alpha}}M^2_{H^+}\right)\right],
\end{aligned} \tag{C.19}$$

$$|\overline{\mathbf{M}}(d_jd_k \to \tilde{u}^*_{i1}H^l_0)|^2 = \frac{g^2\lambda''^2_{ijk}(N_c-1)!}{4N_c}\times$$

Coefficient	
$H^1_{\tilde{d}_{i\alpha}\tilde{d}_{i\beta}}$	$-\frac{M_Z\sin(\alpha+\beta)}{\cos\theta_w}\left[Q^{2i-1}_{1\alpha}Q^{2i-1}_{1\beta}(\frac{1}{2}+e_d\sin^2\theta_w)-e_d\sin^2\theta_w Q^{2i-1}_{2\alpha}Q^{2i-1}_{2\beta}\right]$ $+\frac{m^2_{d_i}\sin\alpha}{M_W\cos\beta}\left[Q^{2i-1}_{1\alpha}Q^{2i-1}_{1\beta}+Q^{2i-1}_{2\alpha}Q^{2i-1}_{2\beta}\right]$ $+\frac{m_{d_i}}{2M_W\cos\beta}(\mu\cos\alpha+A_{d_i}\sin\alpha)\left[Q^{2i-1}_{2\alpha}Q^{2i-1}_{1\beta}+Q^{2i-1}_{1\alpha}Q^{2i-1}_{2\beta}\right]$
$H^1_{\tilde{u}_{i\alpha}\tilde{u}_{i\beta}}$	$\frac{M_Z\sin(\alpha+\beta)}{\cos\theta_w}\left[Q^{2i}_{1\alpha}Q^{2i}_{1\beta}(\frac{1}{2}-e_u\sin^2\theta_w)+e_u\sin^2\theta_w Q^{2i}_{2\alpha}Q^{2i}_{2\beta}\right]$ $-\frac{m^2_{u_i}\cos\alpha}{M_W\sin\beta}\left[Q^{2i}_{1\alpha}Q^{2i}_{1\beta}+Q^{2i}_{2\alpha}Q^{2i}_{2\beta}\right]$ $-\frac{m_{u_i}}{2M_W\sin\beta}(\mu\sin\alpha+A_{u_i}\cos\alpha)\left[Q^{2i}_{2\alpha}Q^{2i}_{1\beta}+Q^{2i}_{1\alpha}Q^{2i}_{2\beta}\right]$
$H^2_{\tilde{d}_{i\alpha}\tilde{d}_{i\beta}}$	$\frac{M_Z\cos(\alpha+\beta)}{\cos\theta_w}\left[Q^{2i-1}_{1\alpha}Q^{2i-1}_{1\beta}(\frac{1}{2}+e_d\sin^2\theta_w)-e_d\sin^2\theta_w Q^{2i-1}_{2\alpha}Q^{2i-1}_{2\beta}\right]$ $-\frac{m^2_{d_i}\cos\alpha}{M_W\cos\beta}\left[Q^{2i-1}_{1\alpha}Q^{2i-1}_{1\beta}+Q^{2i-1}_{2\alpha}Q^{2i-1}_{2\beta}\right]$ $+\frac{m_{d_i}}{2M_W\cos\beta}(\mu\sin\alpha-A_{d_i}\cos\alpha)\left[Q^{2i-1}_{2\alpha}Q^{2i-1}_{1\beta}+Q^{2i-1}_{1\alpha}Q^{2i-1}_{2\beta}\right]$
$H^2_{\tilde{u}_{i\alpha}\tilde{u}_{i\beta}}$	$-\frac{M_Z\cos(\alpha+\beta)}{\cos\theta_w}\left[Q^{2i}_{1\alpha}Q^{2i}_{1\beta}(\frac{1}{2}-e_u\sin^2\theta_w)+e_u\sin^2\theta_w Q^{2i}_{2\alpha}Q^{2i}_{2\beta}\right]$ $-\frac{m^2_{u_i}\sin\alpha}{M_W\sin\beta}\left[Q^{2i}_{1\alpha}Q^{2i}_{1\beta}+Q^{2i}_{2\alpha}Q^{2i}_{2\beta}\right]$ $+\frac{m_{u_i}}{2M_W\sin\beta}(\mu\sin\alpha-A_{u_i}\cos\alpha)\left[Q^{2i}_{2\alpha}Q^{2i}_{1\beta}+Q^{2i}_{1\alpha}Q^{2i}_{2\beta}\right]$
$H^3_{\tilde{d}_{i\alpha}\tilde{d}_{i\beta}}$	$-\delta_{\alpha\neq\beta}\frac{m_{d_i}}{2M_W}(\mu+A_{d_i}\tan\beta)$
$H^3_{\tilde{u}_{i\alpha}\tilde{u}_{i\beta}}$	$-\delta_{\alpha\neq\beta}\frac{m_{u_i}}{2M_W}(\mu+A_{u_i}\cot\beta)$
$H^c_{\tilde{u}_{i\alpha}\tilde{d}_{i\beta}}$	$\frac{1}{\sqrt{2}M_W}\left[Q^{2i}_{1\alpha}Q^{2i-1}_{1\beta}\left(m^2_{d_i}\tan\beta+m^2_{u_i}\cot\beta-M^2_W\sin 2\beta\right)\right.$ $+Q^{2i}_{2\alpha}Q^{2i-1}_{2\beta}m_{u_i}m_{d_i}(\cot\beta+\tan\beta)$ $\left.+Q^{2i}_{1\alpha}Q^{2i-1}_{2\beta}m_{d_i}(\mu+A_{d_i}\tan\beta)+Q^{2i}_{2\alpha}Q^{2i-1}_{1\beta}m_{u_i}(\mu+A_{u_i}\cot\beta)\right]$

Table 8: Higgs couplings to Squarks.

$$\times\left[\sum_{\alpha=1,2}|Q^{2i}_{2\alpha}|^2|H^l_{\tilde{u}_{i\alpha}\tilde{u}_{i1}}|^2\hat{s}R(\tilde{u}_{i\alpha},\hat{s})+2Q^{2i}_{21}Q^{2i}_{22}H^l_{\tilde{u}_{i1}\tilde{u}_{i1}}H^l_{\tilde{u}_{i2}\tilde{u}_{i1}}\hat{s}S(\tilde{u}_{i1},\tilde{u}_{i2},\hat{s},\hat{s})+\right.$$
$$\left.+\frac{|Q^{2i}_{21}|^2|D^l_j|^2}{\hat{t}^2}\left(\hat{u}\hat{t}-M^2_{\tilde{u}_{i1}}M^2_{H^l_0}\right)+\frac{|Q^{2i}_{21}|^2|D^l_k|^2}{\hat{u}^2}\left(\hat{u}\hat{t}-M^2_{\tilde{u}_{i1}}M^2_{H^l_0}\right)\right], \qquad \text{(C.20)}$$

$$|\overline{\mathbf{M}}(u_i d_k\to\tilde{d}^*_{j1}H^l_0)|^2=\frac{g^2\lambda''^2_{ijk}(N_c-1)!}{4N_c}\times$$
$$\times\left[\sum_{\alpha=1,2}|Q^{2j-1}_{2\alpha}|^2|H^l_{\tilde{d}_{j\alpha}\tilde{d}_{j1}}|^2\hat{s}R(\tilde{d}_{j\alpha},\hat{s})+2Q^{2j-1}_{21}Q^{2j-1}_{22}H^l_{\tilde{d}_{j1}\tilde{d}_{j1}}H^l_{\tilde{d}_{j2}\tilde{d}_{j1}}\hat{s}S(\tilde{d}_{j1},\tilde{d}_{j2},\hat{s},\hat{s})+\right.$$
$$\left.+\frac{|Q^{2j-1}_{21}|^2|U^l_i|^2}{\hat{t}^2}\left(\hat{u}\hat{t}-M^2_{\tilde{d}_{j1}}M^2_{H^l_0}\right)+\frac{|Q^{2j-1}_{21}|^2|D^l_k|^2}{\hat{u}^2}\left(\hat{u}\hat{t}-M^2_{\tilde{d}_{j1}}M^2_{H^l_0}\right)\right]. \qquad \text{(C.21)}$$

The coefficients for the various processes can be found in tables 6 and 8.

References

[1] A.K. Grant, R.D. Peccei, T. Veletto and K. Wang, *Speculations on ALEPH's dijet enhancement*, *Phys. Lett.* **B 379** (1996) 272 [hep-ph/9601392].

[2] H. Dreiner, S. Lola and P. Morawitz, *Chargino pair production at LEP2 with broken R-parity: 4-jet final states*, *Phys. Lett.* **B 389** (1996) 62 [hep-ph/9606364].

[3] M. Carena, G.F. Giudice, S. Lola and C.E. M. Wagner, *Four-jet signal at LEP2 and supersymmetry*, *Phys. Lett.* **B 395** (1997) 225 [hep-ph/9612334].

[4] P.H. Chankowski, D. Choudhury and S. Pokorski, *Aleph four-jet excess, R_b and R-parity violation*, *Phys. Lett.* **B 389** (1996) 677 [hep-ph/9606415].

[5] D. Choudhury and D.P. Roy, *An R-parity breaking SUSY solution to the R_b and aleph anomalies*, *Phys. Rev.* **D 54** (1996) 6797 [hep-ph/9608264].

[6] H. Dreiner and P. Morawitz, *High Q^2-anomaly at HERA and supersymmetry*, *Nucl. Phys.* **B 503** (1997) 55 [hep-ph/9703279].

[7] G. Altarelli, J. Ellis, G.F. Giudice, S. Lola and M.L. Mangano, *Pursuing interpretations of the HERA large-Q^2 data*, *Nucl. Phys.* **B 506** (1997) 3 [hep-ph/9703276].

[8] D. Choudhury and S. Raychaudhuri, *R-parity violation at HERA?*, *Phys. Lett.* **B 401** (1997) 54 [hep-ph/9702392].

[9] J. Kalinowski, R. Ruckl, H. Spiesberger and P.M. Zerwas, *Leptoquark/squark interpretation of hera events: virtual effects in e^+e^- annihilation to hadrons*, *Z. Physik* **C 74** (1997) 595 [hep-ph/9703288].

[10] H. Dreiner, *An introduction to explicit R-parity violation*, hep-ph/9707435;
G. Bhattacharyya, *A brief review of R-parity-violating couplings*, hep-ph/9709395.

[11] B.C. Allanach, A. Dedes and H.K. Dreiner, *Bounds on R-parity violating couplings at the weak scale and at the GUT scale*, *Phys. Rev.* **D 60** (1999) 075014 [hep-ph/9906209].

[12] J. Ellis, J.S. Hagelin, D.V. Nanopoulos, K. Olive and M. Srednicki, *Supersymmetric relics from the big-bang*, *Nucl. Phys.* **B 238** (1984) 453.

[13] H. Dreiner and G.G. Ross, *R-parity violation at hadron colliders*, *Nucl. Phys.* **B 365** (1991) 597.

[14] R. Barbier et al., *Report of the group on the R-parity violation*, hep-ph/9810232.

[15] B. Allanach et al., *Searching for R-parity violation at Run-II of the Tevatron*, hep-ph/9906224.

[16] F.E. Paige, S.D. P. pescu, H. Baer and X. Tata, *ISAJET 7.40: a Monte Carlo event generator for pp, $\bar{p}p$ and e^+e^- reactions*, hep-ph/9810440.

[17] G. Corcella et al., *HERWIG 6.1 release note*, hep-ph/9912396;
G. Marchesini et al., *Herwig: a Monte Carlo event generator for simulating hadron emission reactions with interfering gluons. version 5.1 - april 1991*, *Comput. Phys. Commun.* **67** (1992) 465.

[18] S. Moretti et al., Cavendish-HEP-98/06.

[19] B.R. Webber, *Monte Carlo simulation of hard hadronic processes*, *Ann. Rev. Nucl. Part. Sci.* **36** (1986) 253.

[20] G. Marchesini and B.R. Webber, *Simulation of QCD jets including soft gluon interference*, *Nucl. Phys.* **B 238** (1984) 1.

[21] G. Marchesini and B.R. Webber, *Monte Carlo simulation of general hard processes with coherent QCD radiation*, *Nucl. Phys.* **B 310** (1988) 461.

[22] G. Marchesini and B.R. Webber, *Simulation of QCD coherence in heavy quark production and decay*, *Nucl. Phys.* **B 330** (1990) 261.

[23] JADE collaboration, *Test of fragmentation models by comparison with three jet events produced in $e^+e^- \to$ hadrons*, *Phys. Lett.* **B 134** (1984) 275; *Comparison of three jet events with QCD shower models*, *Phys. Lett.* **B 157** (1985) 340;
TPC/Two Gamma collaboration, *Tests of models for quark and gluon fragmentation in e^+e^- annihilation $\sqrt{s} = 29\ GeV$*, *Z. Physik* **C 28** (1985) 31;
Opal collaboration, *A model independent observation of the string effect using quark tagging at LEP*, *Phys. Lett.* **B 261** (1991) 334; *Investigation of the string effect using final state photons*, *Z. Physik* **C 68** (1995) 531.

[24] D0 collaboration, *Color coherent radiation in multijet events from $p\bar{p}$ collisions at $\sqrt{s} = 1.8\ TeV$*, *Phys. Lett.* **B 414** (1997) 419 [hep-ex/9706012].

[25] CDF collaboration, F. Abe et al., *Evidence for color coherence in $p\bar{p}$ collisions at $\sqrt{S} = 1.8\ TeV$*, *Phys. Rev.* **D 50** (1994) 5562.

[26] I.G. Knowles, *A linear algorithm for calculating spin correlations in hadronic collisions*, *Comput. Phys. Commun.* **58** (1990) 271;
Spin correlations in parton-parton scattering, *Nucl. Phys.* **B 310** (1988) 571;
Angular correlations in QCD, *Nucl. Phys.* **B 304** (1988) 767.

[27] K. Odagiri, *Color connection structure of (supersymmetric) QCD ($2 \to 2$) processes*, *J. High Energy Phys.* **10** (1998) 006 [hep-ph/9806531].

[28] B.R. Webber, *A QCD model for jet fragmentation including soft gluon interference*, *Nucl. Phys.* **B 238** (1984) 492.

[29] M.J. Gibbs, A. Ringwald, B.R. Webber and J.T. Zadrozny, *Monte Carlo simulation of baryon and lepton number violating processes at high-energies*, *Z. Physik* **C 66** (1995) 285 [hep-ph/9406266].

[30] J.L. Hewett and T.G. Rizzo, *Resonant slepton production at hadron colliders in R-parity violating models*, hep-ph/9809525.

[31] S. Dimopoulos, R. Esmailzadeh, L.J. Hall and G.D. Starkman, *Cross-sections for lepton and baryon number violating processes from supersymmetry at $p\bar{p}$ colliders*, *Phys. Rev.* **D 41** (1990) 2099;
A. Datta, J.M. Yang, B.-L. Young and X. Zhang, *Effects of R-parity-violating supersymmetry in single top production at the Tevatron*, *Phys. Rev.* **D 56** (1997) 3107 [hep-ph/9704257];
J.-M. Yang et al., *Top quark at the upgraded Tevatron to probe new physics*, hep-ph/9802305;
R.J. Oakes, K. Whisnant, J.M. Yang, B.-L. Young and X. Zhang, *Single top quark production as a probe of R-parity-violating SUSY at pp and $p\bar{p}$ colliders*, *Phys. Rev.* **D 57** (1998) 534 [hep-ph/9707477];
E.L. Berger, B.W. Harris and Z. Sullivan, *Single-top-squark production via R-parity-violating supersymmetric couplings in hadron collisions*, *Phys. Rev. Lett.* **83** (1999) 4472 [hep-ph/9903549].

[32] B.C. Allanach, H. Dreiner, P. Morawitz and M.D. Williams, *Single sneutrino/slepton production at LEP2 and the NLC*, *Phys. Lett.* **B 420** (1998) 307 [hep-ph/9708495].

[33] H.E. Haber and G.L. Kane, *The search for supersymmetry: probing physics beyond the standard model*, *Phys. Rep.* **117** (1985) 75.

[34] J.F. Gunion and H.E. Haber, *Higgs bosons in supersymmetric models, 1*, *Nucl. Phys.* **B 272** (1986) 1.

[35] H. Baer, J. Sender and X. Tata, *The search for top squarks at the Fermilab Tevatron collider*, *Phys. Rev.* **D 50** (1994) 4517 [hep-ph/9404342].

[36] S. Dawson, *R-parity breaking in supersymmetric theories*, *Nucl. Phys.* **B 261** (1985) 297.

[37] J. Butterworth and H. Dreiner, *R-parity violation at HERA*, *Nucl. Phys.* **B 397** (1993) 3 [hep-ph/9211204].

[38] H. Dreiner and P. Morawitz, *Signals for supersymmetry at HERA*, *Nucl. Phys.* **B 428** (1994) 31 [hep-ph/9405253].

[39] E.A. Baltz and P. Gondolo, *Neutralino decay rates with explicit R-parity violation*, *Phys. Rev.* **D 57** (1998) 2969 [hep-ph/9709445].

[40] Particle data group, *Review of particle physics*, *Eur. Phys. J.* **C 3** (1998) 1.